Fast Power Reserve Provision Shift from Conventional Sources to a Battery Energy Storage System: A Deep Learning – Based Control

Antonella Tannous, Reza Razi, Ferréol Binot, Bruno Francois

Univ. Lille, Arts et Métiers Institute of Technology, Centrale Lille, Junia, ULR 2697 - L2EP
F-59000 Lille, France
{antonella.tannous, ferreol.binot, bruno.francois}@centralelille.fr, reza.razi@ensam.eu

***Abstract*— Decarbonizing the energy sector requires integrating intermittent renewable energy sources. Such intermittency increases dependence on costly and environmentally detrimental power reserves provided by fast conventional generators. To maintain grid balance while keeping the energy cheap and decarbonized, grid operators must leverage flexible assets and make swift decisions. This paper introduces a novel deep learning-based controller to manage power reserves from an energy storage system. A deep neural network, trained on real-world data simulated through a physics-based tool, predicts power reserves to address rapid fluctuations. In supplementary to frequency droop controller, the intelligent controller regulates the frequency based on measured or forecasted power inputs. By combining predictive intelligence with real-time fast responsiveness, the proposed framework effectively manages the supply and demand fluctuations, enhancing grid stability while supporting decarbonization and cost efficiency. The framework is validated on an islanded microgrid through an innovative real-time structure using OPAL-RT and SPHEREA simulators.**

Keywords*— Grid balancing, Renewable energy sources, Energy storage, Deep learning, Real-time simulators.

I. Introduction

Over the years, traditional bulk power grids characterized by large conventional predictable and easily operated generators, as well as predictable demand, employ automated processes in control rooms to operate ahead of real-time. These processes are based on the swing equation, which models the power exchange between the mechanical rotor of synchronous generators and electrical grid. Therefore, explicit description of the physics-based mathematical functions and sensitive identification of parameters is unavoidable [1].

The COP28 World Climate Action Summit emphasized the importance of decarbonizing energy sources of bulk power grids to help limit the mean global temperature rise to 1.5°C [2]. This decarbonization effort has led to a growing penetration of intermittent renewable energy sources (RES) at the distribution level, reflecting the distributed and intermittent nature of their resource availability. Additionally, decarbonization has also impacted the demand side, which now features greater variability and unpredictability due to the growing adoption of electric vehicles and battery systems. These new highly uncertain technologies integrated on both sides of the grid are inverter-interfaced technologies that reduce the overall grid's inertia and heightens the susceptibility to power imbalances and fast frequency drops [3]. As power grids become further complex and non-linear systems to operate, their dynamics are pushed closer to their operational limits, and their system parameters are not always accessible. Consequently, traditional model-based control schemes struggle to capture the grid's rapid dynamics and stochastic behaviour, as they rely on accurate system representation and parameter identification [4].

To address these challenges, it is essential to implement flexible system operations that enhance traditional physics-based approaches through continuous adaptive decision-making, to maintain grid balance at minimum economic and environmental costs. This requires leveraging model-free control approaches to enable efficient decisions, minimizing dependence on complex and hard-to-tune models.

As the world witnesses faster and easier access to data collected via smart metering devices along with increased computational capabilities, the adoption of machine learning (ML) methods in power grids is rapidly gaining momentum [5]. For active power balancing in microgrids, ML has emerged as a valuable tool for identifying system models, tuning controller parameters, generating supplementary control signals, or even replacing traditional model-based controllers entirely. Among ML approaches, reinforcement learning (RL) has been extensively applied due to its ability to learn through trial and error. This characteristic enables RL to handle the nonlinear, high-dimensional, and complex nature of microgrid control systems without requiring extensive offline datasets. For instance, [6] demonstrated the use of RL to replace model-based controllers, effectively reducing frequency deviations cause by wind power fluctuations, while other studies have explored its application in generating supplementary control signals for secondary frequency control [7, 8, 9]. However, RL faces several significant challenges such as scalability, as it is prone to the curse of dimensionality and increased complexity in exploration and training. Stability is another concern, with RL algorithms often exhibiting instability due to excessive exploration during learning. Additionally, issues related to the environment, security, and generalization further complicate the deployment of RL for microgrid control [10]. Moreover, RL can be challenging to implement and computationally expensive, particularly in real-time applications.

In contrast, supervised learning provides a more computationally efficient and stable alternative in certain scenarios. It has been extensively applied for fine-tuning frequency controller parameters [11]. Recent studies have explored the use of artificial neural networks (ANN) to fine-tune the inertia of a voltage source converter, enhancing frequency stability [12]. Authors in [13] developed an ANN-based controller to emulate the dynamics of a virtual synchronous generator to control the frequency. Most of these methods overlook the underlying causes of imbalances and rely solely on frequency measurements to balance the grid.

This work has been achieved within the framework of EE4.0 (Energie Electrique 4.0) project. EE4.0 is co-financed by European Union with the financial support of the European Regional Development Fund (ERDF), French State and the French Region of Hauts-de-France.

This paper overcomes the limitations of our previous work [14, 15] by introducing a deep learning-based controller designed to manage uncertainties in power production and demand within a microgrid. The proposed controller operates under realistic conditions, optimize operating costs and reducing CO_2 emissions. More specifically, a deep neural network (DNN)-based controller is developed and trained to predict power reserves at 5-minute intervals with 1-minute resolution. Leveraging power measurements or forecasts, it dynamically substitutes fuel-based power reserves with energy storage-based reserves, ensuring sustainable and efficient microgrid operation. The main contributions of this paper are as follows:

- Development of a real-time DNN-based control approach leveraging measured or very short-term forecasted power, instead of frequency measurements.
- Local integration of the intelligent controller alongside frequency droop control to achieve active power balancing in an islanded microgrid, enhancing system stability and performance.
- Quantitative evaluation of economic and environmental cost savings, achieved by efficiently managing power reserves from an energy storage system.
- Validation of the proposed control framework through an innovative setup using OPAL-RT and SPHEREA code execution hardware platforms.

The remainder of this paper is structured as follows. Section II presents a comprehensive overview of the proposed methodology. Section III details the case study employed for data collection and framework validation. Section IV describes the development and implementation of the proposed control framework. Section V focuses on the methodology for photovoltaic and load power forecasting. In Section VI, the performance assessment metrics for evaluating the proposed control framework are defined. Section VII provides an analysis and discussion of framework's results. Section VIII validates the outcomes through the real-time structure. Finally, Section IX concludes the paper with key insights and an outlook on future work.

II. Overview of The Proposed Methodology

Building trustworthy ML models involves addressing challenges in dataset creation and pre-processing, model training, assessment, and embedding, which can be tackled by integrating solutions into a comprehensive workflow [16].

Our general overview of the proposed methodology is described in Fig. 1. The proposed methodology follows a comprehensive workflow for developing and validating a DNN-based control solution for grid balancing. It begins with offline simulation, where a physics-based domain simulation of an islanded microgrid is conducted to generate a representative dataset (see Section III). This dataset undergoes sampling and pre-processing to ensure it is suitable for DNN model training (see Section IV.B). The next stage focuses on the design of the algorithm, involving hyper-parameter tuning, best model selection, and performance assessment to develop a robust control solution (see Sections IV.C and IV.D). In the online phase (see Section IV.A), the trained DNN model is implemented, in supplementary to the frequency droop control, for active power balancing. While the frequency droop control ensures frequency containment reserves (FCR), the DNN-based controller provides supplementary fast power reserves (secondary control). The DNN-based controller makes predictions of the supplementary minute-by-minute power reserves every 5 minutes, based on measured or forecasted power data (see Section V). Finally, the

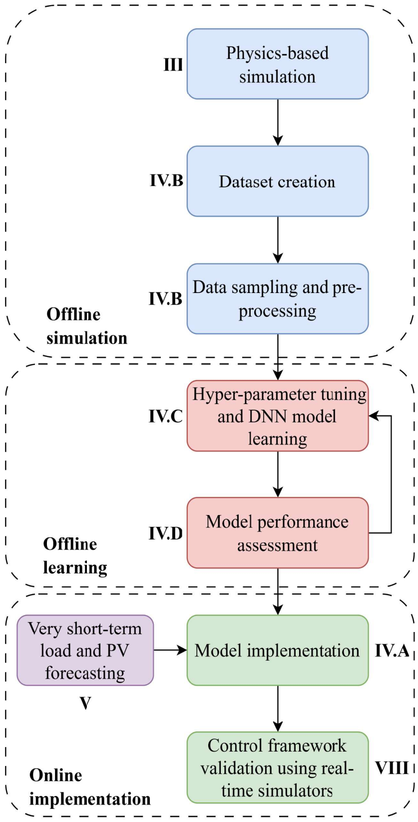

Fig. 1. General overview of the proposed methodology

methodology is rigorously validated using real-time simulators, to evaluate the effectiveness and reliability of the proposed control framework (see Section VIII).

III. Case Study: An Islanded Microgrid

The case study section is structured in two parts. The first part describes the microgrid configuration under study, while the second part specifies the data used for simulation.

A. *Microgrid architecture*

A simulation model of an islanded microgrid was developed on MATLAB/Simulink. The purpose of the simulation model is to 1) provide a database for the training phase and 2) test the proposed control strategy. The architecture of the microgrid is illustrated in Fig. 2. It consists of three layers: the physical, information, and control layers. The physical layer includes a 125 kW 3-phase Diesel Generator (DG), a 50 kW/kWh Li-ion Battery Energy Storage System (BESS), a 42.5 kW Photovoltaic (PV) system, and a group of residential loads with a peak electrical power of 85 kW. The information layer comprises smart meters that monitor and transmit data on PV generation, DG, and residential load power to the energy management system of the BESS. The control layer incorporates droop controllers to deliver FCR using both the DG and the BESS. Additionally, this layer features the proposed intelligent controller responsible for sending control signals to the BESS to ensure the provision of fast power reserves.

B. *PV and load power data*

The simulation is performed by using 186 days of historical PV and residential load data. The dataset is uniformly resampled to a consistent time resolution of one minute, with missing measurements addressed through polynomial interpolation. The PV power production data originates from a PV system installed

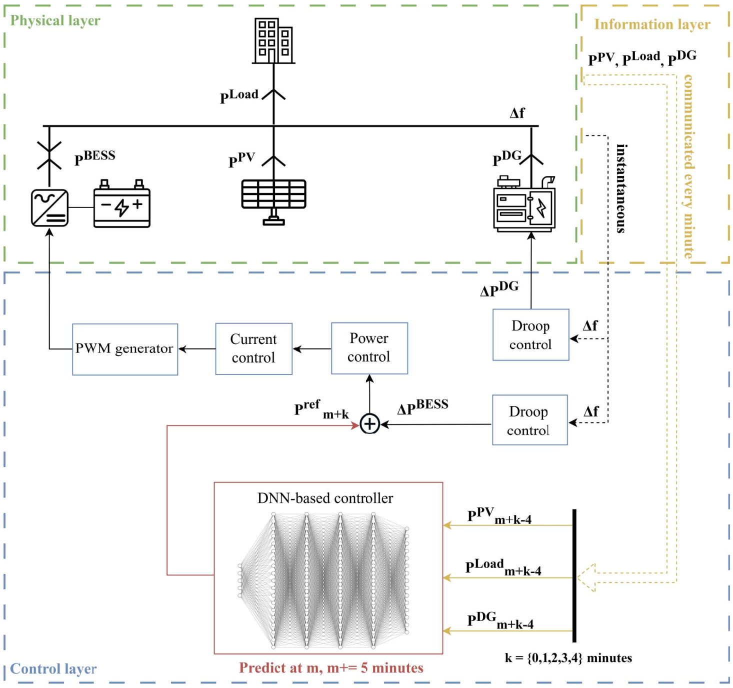

Fig. 2. The physical, information, and control layers of the microgrid

in northern France. This system experiences significant power fluctuations caused by fast-moving clouds. For the residential electrical load, the simulation incorporates the demand profile derived from [17]. Fig. 3 illustrates the PV and load profile on a random day.

IV. Proposed Control Framework

A. *Brief overview of the proposed control framework*

The proposed control framework (see Fig. 2) integrates a DNN-based controller supplementary to physics-based controllers to ensure active power balancing within the microgrid. Instantaneous FCR are provided by both the BESS and DG units through their frequency droop controllers (physics-based). These controllers, based on measured frequency deviation Δf and the same droop coefficient, instantaneously direct the allocation of power reserves ΔP^{DG} and ΔP^{BESS} from the DG and BESS units, respectively. The DNN-based controller utilizes as inputs minutely power measurements of PV, DG and load (P^{PV}_{m+k-4}, P^{DG}_{m+k-4}, and P^{load}_{m+k-4} with $k = \{0, 1, 2, 3, 4\}$ minutes), from 5 minutes prior the time of prediction m. Performance testing has also been conducted using short-term forecasted PV and load power values instead of

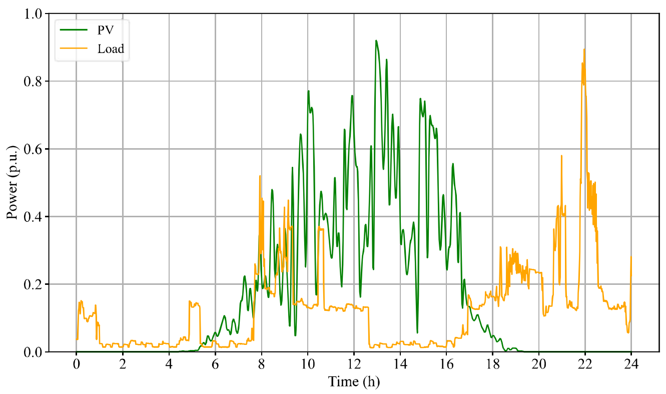

Fig. 3. PV and load demand profile on a random cloudy day

the measurements. Our DNN-based controller forecasts, at the minute m, the next 5 power reference values P^{ref}_{m+k} for the BESS, providing minute-by-minute predictions for the subsequent 5-minute interval. These forecasts are updated every 5 minutes, enabling dynamic scheduling of fast power reserves in the short term. Integrated into the energy management system of the BESS, the DNN-based controller anticipates fluctuations in PV and load power, substituting DG power reserves with BESS power reserves as needed. By offering a more reliable and flexible energy reserve, the controller enhances microgrid stability, reduces CO_2 emissions and operational costs.

B. *Data creation, sampling and pre-processing*

Supervised learning algorithms, such as deep learning, depend on datasets derived from either measurements or simulations. Simulation-based data generation provides the flexibility to create extensive datasets but is constrained by computational demands, particularly in non-linear systems or high-dimensional feature spaces [18]. As dimensionality increases, the sample size required for comprehensive coverage grows exponentially. To address this, targeted input selection can reduce the need for exhaustive sampling by focusing on outputs of interest.

In this study, the training process for the DNN leverages a simulation-based dataset comprising input and target values. The dataset is generated by simulating the same microgrid with fluctuating load and PV power inputs, deliberately excluding the BESS. This exclusion allows the DNN to learn the DG control policy in response to variations in load and PV power. The simulation spans 186 representative days with a 1-minute timestep to capture rapid fluctuations throughout the day and across different seasons.

The DNN within the BESS control system is designed to emulate the DG's droop controller during slow transients. To achieve this, the DNN is trained on the DG's slow power transient responses ΔP^{DG} sampled every minute, using input features f including PV power P^{PV}, load power P^{load}, and DG

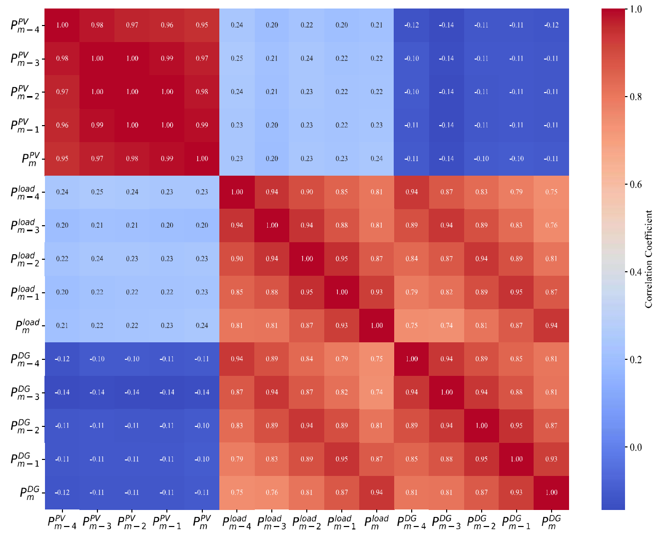

Fig. 4. Correlation study between input features

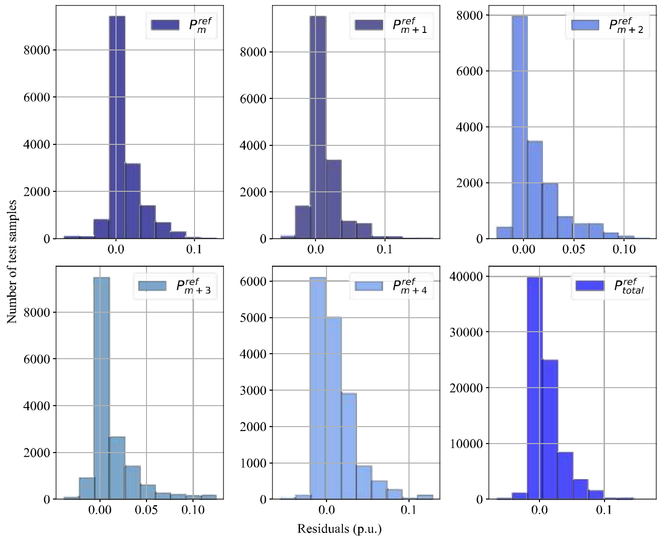

Fig. 5. Residual distribution of predicted output for test samples

power P^{DG}. These inputs enable the DNN to model the droop controller's behaviour under varying conditions effectively.

Fig. 4 depicts the correlation between the input features. The diesel generator power P^{DG} shows a strong correlation (red – closer to 1) with P^{load} highlighting its key role in balancing demand when P^{PV} is insufficient. In contrast, P^{PV} exhibits weaker correlations (blue – closer to 0) with both P^{load} and P^{DG} because PV generation occurs only during daylight hours and is zero outside this period. However, both P^{PV} and P^{load} demonstrate strong temporal correlations within their respective time series, reflecting smooth and predictable very short-term trends (see Section V).

Prior to training, the dataset undergoes pre-processing. A 70/30 training-testing split is applied with a fixed random seed to ensure consistent conditions across models. Validation data, constituting 20% of training data, is crucial for assessing generalization and selecting optimal models. Pre-processing steps include standardizing input and target data, formatting to seven decimal places for precision, and handling the absence of values in the simulation-generated dataset.

C. Hyper-parameter tuning and DNN model selection

Overfitting occurs when a model performs well on training data but poorly on unseen data. To mitigate this, we monitor the validation error during training. Techniques include early stopping, where training halts if validation performance stops improving, and regularization (e.g., L1 or L2 penalties) to constrain model complexity and improve generalization. Additionally, hyperparameter tuning—adjusting parameters like model size, optimizer settings, or regularization strength—further enhances performance. Since hyperparameters affect model generalization in complex ways, they are typically optimized by using methods such as random search, grid search, Bayesian optimization, etc. [19].

Unlike grid search, which evaluates all possible combinations, random search explores a subset of configurations. Random search often leads to better results in less time, especially for high-dimensional parameter spaces.

In this study, we have chosen random search to explore the hyperparameter space by randomly sampling different combinations, evaluating up to 50 trials where each trial represents a unique set of hyperparameters (see Table I). During each trial, the model is trained on the training dataset and validated on a subset, with performance measured by the validation loss after each epoch. The best hyperparameters are retrieved based on the lowest validation loss across all trials. The best model architecture (see Table II) is rebuilt using the best hyperparameters.

D. DNN model training and performance assessment

Once the best model architecture is determined, the training process involves optimizing the model's weights and biases to minimize the loss function, thereby enhancing its predictive accuracy. The training process uses the Adam optimizer, which adapts the learning rates for each parameter, enhancing convergence. Additionally, the learning rate is dynamically reduced by 10% after 10 epochs to refine adjustments during later stages of training. Training is capped at 100 epochs but early stopping halts the process if the validation loss does not improve for 5 consecutive epochs, preventing overfitting. The resulting weights and biases represent the final learned parameters, which the model uses to make predictions. The mean squared error MSE is favoured for its ability to heavily penalize large errors, making the model more sensitive to significant deviations. The performance of the training and validation processes is assessed by using MSE, as defined in (1):

Table I HYPER-PARAMETER OPTIONS

Hyper-parameter	Options
Number of layers	[3, 6] step size: 1
Nodes per layer	[16, 192] step size: 16
Activation function	Linear, ReLU, leaky ReLU, tanh, sigmoid
Leaky ReLU α	[0.01,0.3] step size: 0.1
Dropout rate	[0.2, 0.5] step size: 0.1
Learning rate	$[10^{-4}, 10^{-2}]$ logarithmic sample

Table II BEST DNN MODEL ARCHITECTURE

Layer Type	Number of Parameters
Dense ReLU	3,072
Batch normalization	768
Dropout 0.4 rate	0
Dense leaky ReLU	18,528
Dense leaky ReLU	9,312
Dense leaky ReLU	9,312
Dense linear	485

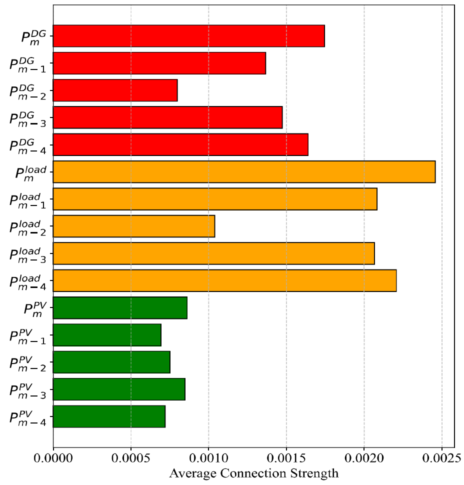

Fig. 6. Bar chart of the average connection strength of each input feature

$$\text{MSE} = \frac{1}{n} \cdot \sum_{i=1}^{n} (y_i - \hat{y}_i)^2 \tag{1}$$

where y_i and $\hat{y}_i$ denote the actual and predicted values, respectively, across the total number of samples n.

After 14 epochs, the training error reaches 0.0009, while the validation error stands at 0.001. A histogram of the test residuals, defined as $y_i - \hat{y}_i$ of the test samples, is illustrated in Fig. 5. The residual distributions for each output P_{m+k}^{ref} (with $k = \{0, 1, 2, 3, 4\}$) are tightly clustered around 0, suggesting the model performs well on unseen test data. Most residuals are slightly positive, suggesting a tendency to underestimate actual values, while the range of residuals spans from –0.05 to 0.15 per unit. The residuals of earlier outputs, such as P_m^{ref} and P_{m+1}^{ref} are more tightly distributed than later outputs, highlighting increased variability in predictions over the prediction horizon. Overall, the residuals for the total test samples P_{total}^{ref} confirm the model's reliability, showing minimal errors and few extreme outliers.

Fig. 6 highlights the impact of each input feature on the outputs through the average connection strength, calculated as the average magnitude of weights associated with each input feature across all connections. The most recent and delayed load power inputs, P_m^{load} and P_{m-4}^{load}, exhibit the highest connection strengths, while P_{m-2}^{load} demonstrates the weakest connection among the load features. This pattern is attributed to the volatile nature of the load demand. Even though PV generation has an important impact on the outputs during daylight hours, the PV power inputs show the lowest average connection strength, reflecting their minimal influence on the outputs, due to the absence of PV power generation outside daylight hours. Consequently, the DG power, which is more influenced by load power than PV power (see Fig. 4), displays moderate impact on the outputs. Fig. 7 further supports this analysis by displaying the dot product of the connection weights between each input and output feature. The colour intensity highlights the relative importance of each input, where warmer colours (yellow) indicate stronger weights. It is evident that P_m^{load} and P_{m-4}^{load} contribute significantly to the predictions $\widehat{P}_m^{ref}$ and $\widehat{P}_{m+4}^{ref}$.

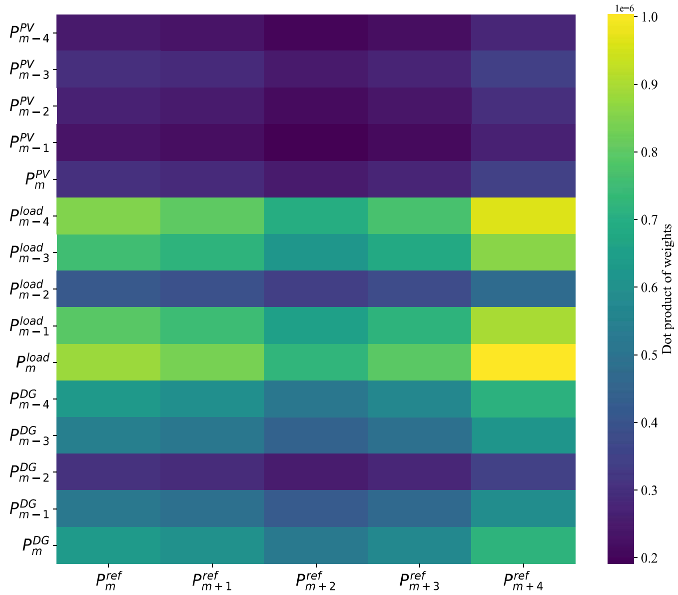

Fig. 7. Dot product of weights for all layers connecting each input feature to the outputs

V. Load and PV Forecasting

Load and PV forecasting is essential for anticipating future energy demands and supply over various time horizons, with very short-term forecasting (VSTF) focusing on predictions ranging from 1 minute to 1 hour ahead. VSTF is crucial for real-time decision-making, addressing very short-term random variations in supply and demand to maintain balance and minimize operational costs.

In this study, very-short term forecasting is performed at the time m to provide minute-by-minute forecasts for the subsequent 5 minutes. The forecasting error is evaluated using the mean absolute error MAE, given by (2):

$$\text{MAE} = \frac{1}{n} \cdot \sum_{i=1}^{n} |y_i - \hat{y}_i| \tag{2}$$

A. *Very short-term load forecasting*

Residential loads are the most challenging to forecast due to their volatility and non-linearity driven by human behaviour, making load VSTF especially difficult. Various methods like Time-Series analysis [20], Long-Short Term Memory [21], Polynomial Regression [22], and other hybrid combinations of methods [23] have been widely employed for VSTF of load demand. In this study, Polynomial Ridge Regression is chosen for its simplicity and computational efficiency. It generates minute-by-minute load predictions $\widehat{P}_{m+k}^{load}$ for the next 5 minutes (with $k = \{0, 1, 2, 3, 4\}$), by leveraging historical data from the previous 5 minutes, specifically P_{m+k-4}^{load}.

Polynomial Ridge Regression is a type of regression technique that combines polynomial feature transformation with L2 regularization (Ridge) to prevent overfitting. By adding a penalty term R to the cost function, Ridge regression helps control the magnitude of the model's coefficients, ensuring its robustness to small fluctuations in the training data compared to standard polynomial regression. The model captures complex relationships in data by using polynomial features described in (3) for each value of k:

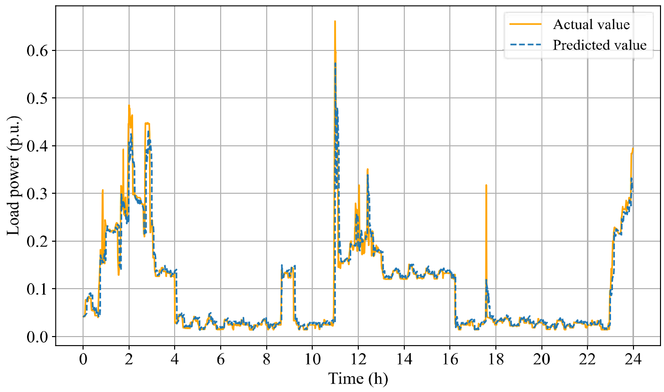

Fig. 8. Actual versus predicted load power on a random day

$$\widehat{P}_{m+k}^{load} = \beta_0 + \sum_{d=1}^{D} \beta_d \cdot (P_{m+k-4}^{load})^d \tag{3}$$

where β_0 is the intercept term, and β_d are the coefficients corresponding to the d-th degree terms in the polynomial of degree D. The hyperparameter D will be next optimized.

The dataset is partitioned as follows: 70% for training (including 10% for validation) and 30 % for testing. A grid search is conducted to identify the optimal hyperparameters for a Polynomial Ridge Regression model. This process involves performing 5-fold cross-validation for each hyperparameter combination, calculating the average negative MSE across all folds. The hyperparameters yielding the lowest average negative MSE are selected as the optimal configuration, minimizing the Polynomial Ridge Regression objective function $L(\beta)$ as described in (4) and (5):

$$L(\beta) = \frac{1}{n} \cdot \sum_{m=5,\, m+5,\, \ldots}^{n} (P_{m+k}^{load} - \widehat{P}_{m+k}^{load})^2 + R \tag{4}$$

where

$$R = \lambda \cdot \sum_{d=1}^{D} \beta_d^{\,2} \tag{5}$$

The analysis identifies a polynomial degree of 3 and a ridge regularization strength λ of 0.01 as the optimal parameters. The values of β_0 and β_d are determined by the regression process itself. The resulting model achieves a MAE of 2% on unseen data. Fig. 8 showcases the actual versus predicted load demand on a random day.

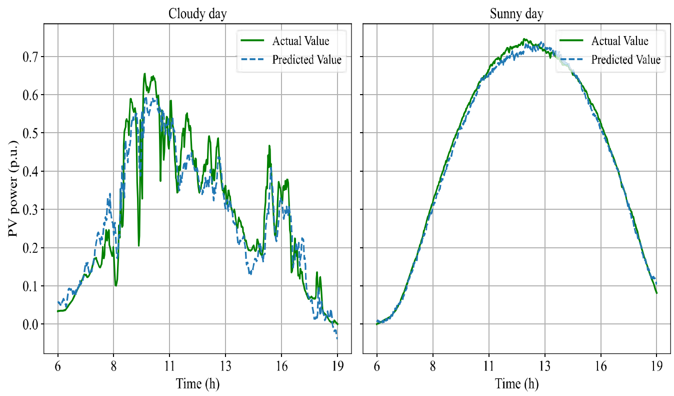

Fig. 9. Actual versus predicted PV power on a cloudy and sunny day

B. *Very short-term Photovoltaic forecasting*

Very short-term solar forecasting, also known as intra-hour solar forecasting, refers to the prediction of PV power generation within the same hour, typically at higher time resolutions such as every 5, 10, or 15 minutes. Several methods have been developed for this task, including time-series models like ARIMA, statistical and machine learning models, and advanced image-based techniques. Recent advances leverage satellite and sky images with convolutional neural networks (CNNs) and long short-term memory networks. Combining ground-based sky imagery with historical PV outputs in specialized CNN architectures has shown promise, particularly for handling complex cloud movements and short prediction horizons [24].

This study builds upon the PV forecasting approach presented in [25], with a key modification reducing the forecasting horizon from 15 minutes to 5 minutes. The proposed hybrid model combines image-based and temporal features using a CNN architecture and fully connected layers. It processes a sequence of images from a 360-degree fisheye camera, concatenated along the colour channel, combined with the measured PV power from 5 minutes prior P_{m+k-4}^{PV}, which is integrated mid-network.

The hybrid model, illustrated in Fig. 10 predicts PV power output $\widehat{P}_{m+k}^{PV}$ for the upcoming 5 minutes by leveraging spatial features from image sequences and numerical PV power data. The input consists of 5 image sequences, each with dimensions 64×64 pixels with 3 color channels RGB (Red-Green-Blue), passed through two convolutional layers with 24 and 48 filters, respectively. Each convolutional layer is followed by batch normalization, ReLU activation, and max pooling. The extracted spatial features are then flattened and concatenated with P_{m+k-4}^{PV}. This fused feature representation is processed through two fully connected layers, each containing 1024 neurons with ReLU

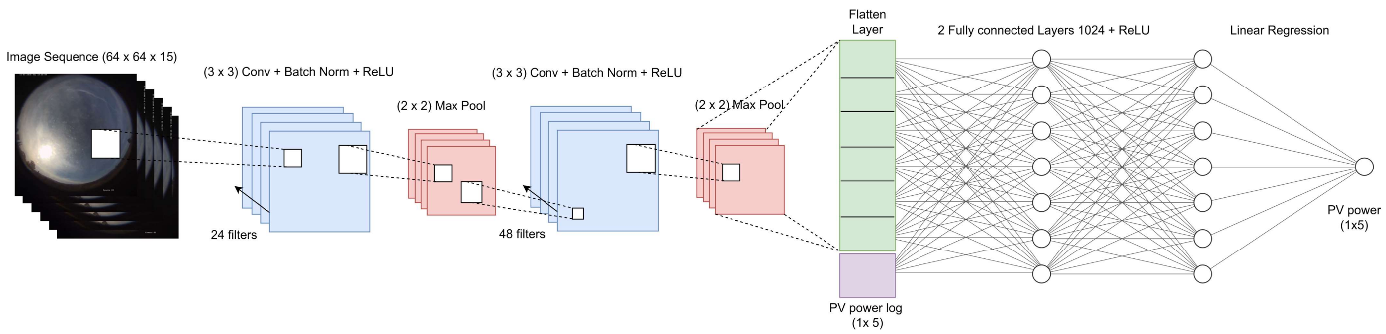

Fig. 10. Hybrid CNN model with PV power log to predict PV power

activation. The model concludes with a linear regression layer to predict PV power outputs $\widehat{P}_{m+k}^{PV}$. The architecture incorporates strong regularization techniques, such as dropout and batch normalization, to enhance generalization and effectively predict short-term PV power variations. The hybrid model achieves a 2.12% MAE on previously unseen sunny days and a 7.78% MAE on previously unseen cloudy days. Fig. 9 showcases the actual versus predicted PV power on a cloudy and sunny day.

VI. PERFORMANCE EVALUATION METRICS

The performance of the proposed control strategy is evaluated over a period T of 5 minutes, through three interrelated metrics: technical, environmental, and economic. The technical performance is assessed by analysing frequency stability using the Integral of Frequency Deviation (IFD). The environmental impact is quantified by calculating the total mass of CO_2 emissions generated during the operation of the DG. Finally, the economic aspect is evaluated by determining the costs incurred from fuel consumption by the DG and the associated taxes on emissions. This integrated evaluation framework ensures a holistic assessment of the control strategy, addressing reliability, sustainability, and cost-efficiency.

A. *Integral of frequency deviation*

The IFD is a robust and intuitive metric for analysing frequency stability in power grids with a high share of RES. The IFD metric, defined in (6), evaluates the cumulative magnitude of the deviation from the nominal frequency $f_{nominal}$ (50 Hz in this case) over the specified period T.

$$\text{IFD} = \int_0^T |f(t) - f_{nominal}|dt \tag{6}$$

B. *Environmental costs*

The operating CO_2 emissions within the microgrid depend on the DG's fuel consumption denoted as l_{fuel} [L/kWh] and can be formulated as a quadratic function of the DG power P^{DG}. The coefficients of this function are determined through curve fitting of the fuel consumption chart [26] (see Table III), as described in (7):

$$l_{fuel} = (-5\times 10^{-4})\cdot {P^{DG}}^2 + 0.3\cdot P^{DG} + 2.4 \tag{7}$$

Given that a DG releases 2.68 kg of CO_2 per Liter of fuel consumed [27], the total emitted mass m_{CO_2} [kg] of CO_2 can be represented by (8). This equation is as a function of DG power evolution, accounting for the engine delay T_e with a specified value of 0.03 seconds [28].

$$m_{CO_2} = \int_0^T 2.68/Te \cdot e^{-t/_{Te}} \cdot l_{fuel}\, dt \tag{8}$$

C. *Economic costs*

The total operating costs c_{eco} can be formulated by incorporating both the cost of consumed diesel and the tax associated with the mass of CO_2 emitted, as depicted in (9). The considered cost of a Liter of diesel is 1.865 €, while the CO_2 emission tax is 44.6 € per ton [3].

$$c_{eco} = 44.6/1000 \cdot m_{CO_2} + 1.865 \cdot \int_0^T l_{fuel}\, dt \tag{9}$$

Table III FUEL CONSUMPTION CHART FOR THE SPECIFIED DG

DG Power [kW]	Fuel Consumption [L/h]
50% load	21.90
75% load	30.30
100% load	37.80

VII. RESULTS AND DISCUSSION

In this section, the proposed control framework is evaluated using an islanded microgrid model developed in MATLAB/Simulink (see Fig. 2). The primary objective is to assess the framework's performance under conditions closely resembling real-world operating conditions, characterized by continuous fluctuations in PV and load power. The evaluation compares the framework, which integrates the DNN-based controller with the BESS and the DG frequency droop controllers, across two scenarios (see Fig. 11): one using historically measured power inputs of Section V (red curve – control scenario 1) and the other using forecasted power inputs (green curve – control scenario 2). The analysis also includes comparisons with a scenario involving only the DG and BESS droop controllers (blue curve – control scenario 3) and another scenario relying solely on the DG droop controller (yellow curve – control scenario 4).

The simulation is carried out over a 10-minute duration. During the initial five minutes, the DNN-based controller does not generate BESS reference power, as historical power measurements are required to initialize its algorithm. These measurements are not available at the start of the simulation and are instead collected during the first 5 minutes. Therefore, the results presented in Fig. 11 focus on the period from 4.5 to 10 minutes only, highlighting the performance of the proposed control framework starting minute 5.

During the initial 5 minutes, only the DG droop controller (yellow curve) responds to the frequency deviation Δf of 0.21 Hz by supplying FCR. In contrast, the red, green, and blue curves state the contribution of both the BESS and DG droop controllers to the frequency regulation according to their

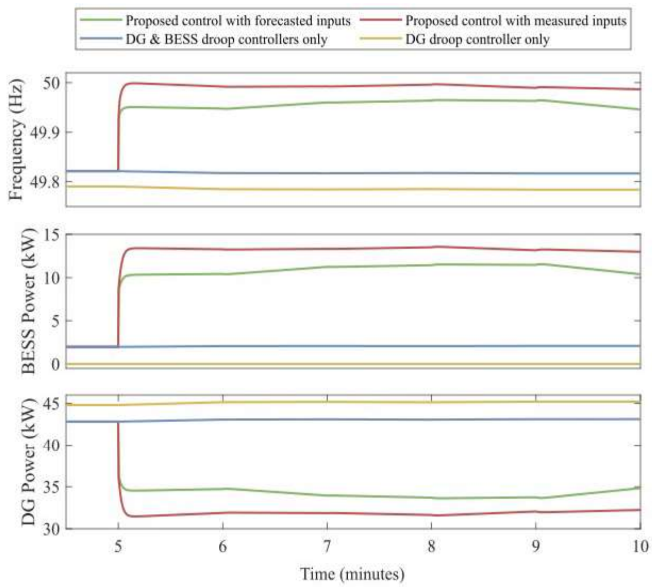

Fig. 11. Microgrid frequency, BESS and DG active power under four control scenarios, for continuously fluctuating PV and load power

respective power capacities and droop coefficients. As expected, the microgrid frequency regulation is more effective when the BESS provides an additional 2 kW of FCR, thereby improving overall system stability. This contribution not only enhances frequency control but also reduces operational costs and emissions by displacing DG-based reserves.

After 5 minutes (m = 5), the DNN-based controller generates five predicted BESS reference values P_{m+5}^{ref} for both the red and green curves. These predictions will increase the provision of supplementary fast power reserves from the BESS, mitigating and replacing the reserves provided by the DG. The VSTF exhibit a total error of 6% on both PV and load power for this test, which affects the accuracy of the DNN's predictions when relying on forecasted power inputs. The DNN-based controller utilizing measured inputs (red curve) outperforms the one using forecasted inputs (green curve). Specifically, the control framework in the red curve most effectively maintains the microgrid frequency closest to 50 Hz, while further minimizing DG power consumption.

Table IV presents the performance evaluation metrics for each scenario over the 5-minute period. The DNN-based controller with measured inputs (control scenario 1) achieves the lowest values for the IFD, m_{CO_2} and c_{eco} metrics. Conversely, scenario 4, which only uses the DG droop controller, exhibits the highest values for these metrics. Scenario 1 reduces the IFD metric by 0.18, 0.87, and 1.04 Hz·min compared to scenarios 2, 3, and 4, respectively. Furthermore, scenario 1 results in a reduction of the mass of CO_2 emissions m_{CO_2} and operating costs c_{eco} by 5.3%, 21.05%, and 30.3% compared to scenarios 2, 3, and 4, respectively.

The DNN-based controller with forecasted inputs demonstrates an improvement in system performance by 0.69 Hz·min and a reduction in costs and emissions by 15.9% compared to scenario 3. Additionally, it shows an improvement of 0.86 Hz·min and a reduction in costs and emissions by 23.7% compared to scenarios 4. However, its effectiveness depends on the accuracy of the forecasted power inputs. Smaller discrepancies between actual power measurements and forecasts

Table IV PERFORMANCE EVALUATION METRICS

Control scenario	IFD [z .min]	m_{CO_2}[kg]	c_{eco} [€]
1 (red curve)	0.04	2.557	1.89
2 (green curve)	0.22	2.693	1.99
3 (blue curve)	0.91	3.214	2.38
4 (yellow curve)	1.08	3.332	2.47

lead to better outcomes for the DNN-based controller in scenario 2. Scenarios 1 and 2 significantly improve on the three indicators used, compared with scenarios 3 and 4. Scenario 1 is indeed the most accurate, but measurements are not always available. The use of load and PV prediction algorithms are therefore good tools for improving the control framework's data input.

VIII. VALIDATION OF THE CONTROL FRAMEWORK USING AN INNOVATIVE REAL-TIME STRUCTURE

The performance and effectiveness of the proposed control framework are validated by using an innovative setup featuring two advanced real-time simulators, interconnected via robust communication protocols, as depicted in Fig. 12. The OPAL-RT simulator is employed to model the physical and control layers of the microgrid using MATLAB/Simulink software. Simultaneously, the SPHEREA simulator is utilized to execute the DNN algorithm for predicting future setpoints, leveraging U-Test software and Python programming for algorithm implementation. A bidirectional communication protocol—Message Queuing Telemetry Transport (MQTT)—ensures seamless and reliable data exchange between the simulators, facilitating the synchronization of their operations.

Every 5 minutes, the OPAL-RT simulator transmits load, PV and DG power measurements to the SPHEREA simulator. The DNN model in SPHEREA predicts the reference power P_{ref} for the next 5 minutes and relays this information to the ESS's control layer.

To visualize and analyse the results in real-time, a Supervisory Control and Data Acquisition (SCADA) system is implemented using PcVue software, which is communicating with the simulators via the Open Platform Communications (OPC) protocol. The SCADA system provides a user-friendly interface with advanced real-time monitoring and analytical

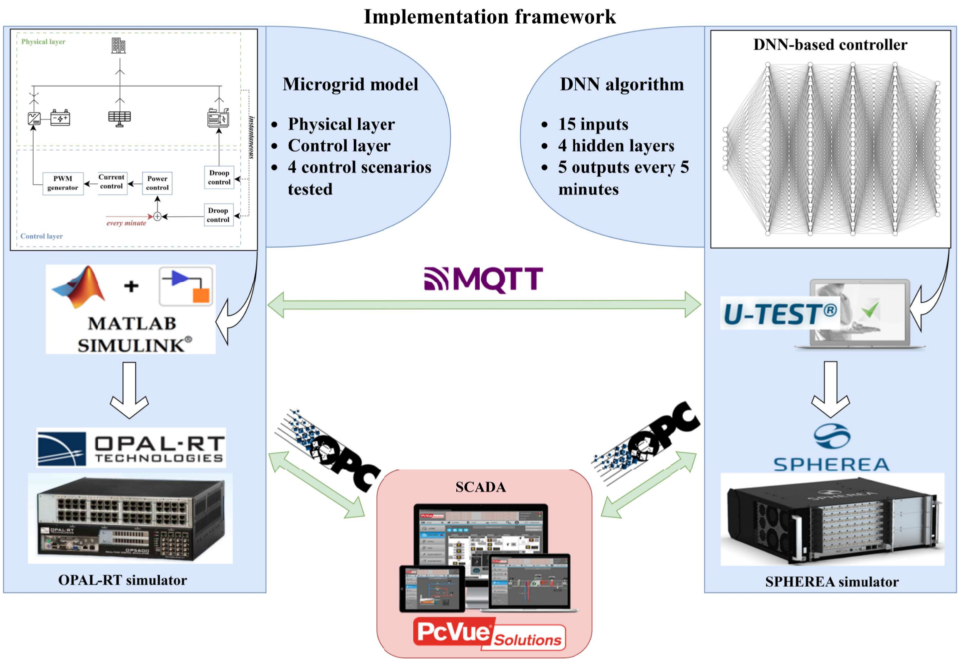

Fig. 12. Hardware and software organization of the real-time structure

capabilities. This interface enables users to observe and adjust the current state of the process dynamically. Key features included:

- Switching between control scenarios for comparative performance evaluation.
- Monitoring critical metrics such as system frequency, as well as the power outputs of DG and BESS units.
- Detailed insights into the evolution of operational parameters, including fuel consumption, associated costs, and emissions for each control strategy.

A key advantage of the real-time simulation environment is its computational efficiency compared to conventional PC-based simulations. While the real-time structure runs simulations at actual system speed, executing the same simulation on a high-performance PC equipped with a 12th Gen Intel® Core™ i7-12700H processor (2.3 GHz) and 32 GB of RAM takes almost eight times longer.

IX. CONCLUSIONS

This paper addresses the challenge of maintaining grid balance amidst the stochastic and intermittent nature of RES and the growing unpredictability of load demand. A novel DNN-based control framework is proposed to dynamically manage power reserves from a BESS, complementing frequency droop controllers. Unlike conventional frequency-based approaches, the DNN-based controller leverages historical power measurements or very short-term forecasts to provide fast, clean, and cost-effective power reserves. The framework is validated using realistic load and PV power profiles within an innovative real-time setup that closely emulates real-world operating conditions.

The proposed approach demonstrates significant advantages in frequency regulation, economic efficiency, and environmental impact. Compared to a control framework that relies solely on droop controllers, the DNN-based controller effectively reduces dependence on the DG, leading to lower CO_2 emissions and operational costs. The results confirm that using historically measured power inputs achieves the most accurate performance, maintaining microgrid frequency closest to 50 Hz while minimizing DG power consumption. Furthermore, the integration of very short-term forecasting provides a viable alternative when real-time measurements are unavailable, highlighting the adaptability of the proposed method.

Despite its promising results, this study has some limitations. The accuracy and reliability of the proposed method depend on the availability and quality of the data used for training and forecasting. Forecasting uncertainty can introduce deviations in power reserve predictions, affecting control performance. Additionally, the framework assumes the availability of sufficient power reserves from the BESS, which may not always be guaranteed under extreme operating conditions. Finally, real-time implementation may face computational constraints, including hardware limitations and communication delays, which require further investigation for large-scale deployment.

As a continuation of this work, we propose an investigation into the use of Importance Sampling to optimize the selection of a sampling distribution, focusing on identifying and prioritizing informative samples [18]. This approach aims to reduce the offline computation time and evaluate whether the DNN can sustain robust performance when trained on a smaller available dataset. Another key aspect is evaluating the controller's ability to maintain grid balance in the absence of conventional droop controllers, thus exploring its potential to operate autonomously under decentralized conditions. Finally, we plan to extend the study to a larger microgrid with multiple distributed RES and energy storage systems, employing a distributed learning approach to enable coordinated control among storage units and ensure grid stability in more complex systems. These directions aim to enhance the scalability, adaptability, and practical applicability of DNN-based controllers.

REFERENCES

[1] O. Stanojev, Y. Guo, . Aristidou, and G. ug, "Multiple Ancillary Services Provision by Distributed Energy Resources in Active Distribution Networks," in *IREP 2022 - 11th Bulk Power Systems Dynamics and Control Symposium*, 2022, pp. 1-11.

[2] *United Nations Framework Convention on Climate Change*. Accessed: Mar. 14, 2024. [Online]. Available: http://unfccc.int/decisions.

[3] M. I. Saleem, S. Saha, and T. K. Roy, "A fre uency stability assessment framework for renewable energy rich power grids," *Sustainable Energy, Grids and Networks*, vol. 38, pp. 101380-101396, 2024.

[4] O. Stanojev, U. Markovic, P. Aristidou, G. Hug, D. Callaway, and E. Vrettos, "M C-Based Fast Frequency Control of Voltage Source Converters in Low-Inertia ower Systems," *IEEE transactions on power systems*, vol. 37, no. 4, pp. 3209–3220, 2022.

[5] A. Tannous, R. Razi, F. inot, and . Francois, "A review of self-learning and adaptive techni ues for grid balancing," in *Symposium de Génie Electrique*, 2023, pp. 1–6.

[6] Z. Yan and Y. Xu, "Data-Driven Load Frequency Control for Stochastic Power Systems: A Deep Reinforcement Learning Method with Continuous Action Search," *IEEE transactions on power systems*, vol. 34, no. 2, pp. 1653–1656, 2019.

[7] M. Adibi and J. Van der oude, "Secondary fre uency control of microgrids: An online reinforcement learning approach," *IEEE Trans. Autom. Control*, vol. 67, no. 9, pp. 4824–4831, Sep. 2022.

[8] M. . Khooban and M. Gheisarnejad, "A novel deep reinforcement learning controller-based type-II fuzzy system: Frequency regulation in microgrids," *IEEE Trans. Emerg. Topics Comput. Intell.*, vol. 5, no. 4, pp. 689–699, Aug. 2021.

[9] A. Venkataramanan and A. Mehrizi-Sani, "Reinforcement Learning-Based Transient Response Shaping for Microgrids," in *IREP 2022 - 11th Bulk Power Systems Dynamics and Control Symposium*, 2022, pp. 1-9.

[10] . She, F. Li, . Cui, J. Zhang, and R. o, "Fusion of Microgrid Control with Model-free Reinforcement Learning: Review and Vision," *IEEE transactions on smart grid*, vol. 14, no. 4, pp. 3232–3245, 2023.

[11] F. abibi, S. Shokoohi, and . evrani, "Designing a self-tuning frequency controller based on ANN for an isolated microgrid," in *Int. Symp. On Smart Grid Operation and Control*, 2012, pp. 1–12.

[12] F. Yao, J. Zhao, X. Li, L. Mao, and K. Qu, "R F Neural Network ased Virtual Synchronous Generator Control with Improved Frequency Stability," *IEEE transactions on industrial informatics*, vol. 17, no. 6, pp. 4014–4024, 2021

[13] H. Issa, V. Debusschere, L. Garbuio, P. Lalanda, and N. Hadjsaid, "Artificial intelligence-based controller for grid-forming inverter-based generators," in *Innovative Smart Grid Technologies Conf.*, 2022, pp. 1–6

[14] A. Tannous, R. Razi, F. inot, . Francois, "Artificial neural network-based fast power reserve control for active power balancing," *Int. Conf. Electrimacs*, 2024, pp. 1–6.

[15] A. Tannous, R. Razi, F. inot, . Francois, "Short-Term Scheduled Power Reserve: An Artificial Neural Network Approach," *CIRED 2024 Vienna Workshop*, 2024, pp. 1–6.

[16] J. Stiasny, S. Chevalier, R. Nellikkath, B. Sævarsson, and S. Chatzivasileiadis, "Closing the Loop: A Framework for Trustworthy Machine Learning in ower Systems," in *IREP 2022 - 11th Bulk Power Systems Dynamics and Control Symposium*, 2022, pp. 1-21.

[17] G. Hebrail and A. Berard. "Individual Household Electric Power Consumption," UCI Machine Learning Repository, 2006. [Online]. Available: https://doi.org/10.24432/C58K54.

[18] C. amon, M. erninge, and L. Söder, "An importance sampling techni ue for probabilistic security assessment in power systems with large amounts of wind power," *Electric power systems research*, vol. 131, pp. 11–18, 2016.

[19] L. Yang and A. Shami, "On hyperparameter optimization of machine learning algorithms: Theory and practice," *Neurocomputing*, vol. 415, pp. 295–316, 2020.

[20] L. C. M. de Andrade and I. N. da Silva, "Very Short-Term Load Forecasting ased on ARIMA Model and Intelligent Systems," in *2009 15th International Conference on Intelligent System Applications to Power Systems*, IEEE, 2009, pp. 1–6.

[21] K. Li, . uang, G. u, and J. Li, “Ultra-short term power load forecasting based on CEEMDAN-SE and LSTM neural network,” *Energy and buildings*, vol. 279, pp. 112666- 112681, 2023.

[22] V. K. Vats, S. Rai, D. harti, and M. De, “Very Short-Term, Short-Term and Mid-Term Load Forecasting for Residential Academic Institute: A Case Study,” in *2018 4th International Conference on Computing Communication and Automation (ICCCA)*, IEEE, 2018, pp. 1–6.

[23] M. Zhang *et al.*, “Accurate ultra-short-term load forecasting based on load characteristic decomposition and convolutional neural network with bidirectional long short-term memory model,” *Sustainable Energy, Grids and Networks*, vol. 35, pp. 101129- 101143, 2023.

[24] Y. Chu, M. Li, C. F. M. Coimbra, D. Feng, and . ang, “Intra-Hour Irradiance Forecasting Techniques for Solar Power Integration: A Review,” *iScience*, vol. 24, no. 10, pp. 1-50, 2021.

[25] Y. Sun, V. Venugopal, and A. R. randt, “Short-term solar power forecast with deep learning: Exploring optimal input and output configuration,” *Solar energy*, vol. 188, pp. 730–741, 2019.

[26] Ministère de l’economie, des finances, et de la souveraineté industrielle et numérique, “Guide 2024 sur la fiscalité des énergies”, pp. 7

[27] Caterpillar Diesel Generator Sets D125 GC. [Online]. Available: http://www.cat.com/en_GB/products/new/power-systems/electric-power/diesel-generator-sets/106020.html.

[28] M. Khursheed, M.A. Mallick, and A. Iqbal, “Performance analysis of closed loop control of diesel generator power supply for base transceiver (BTS) load,” *International Journal of Innovative Technology and Exploring Engineering (IJITEE)*, vol. 8, pp. 2483-2495, 2019.

Fast Power Reserve Provision Shift from Conventional Sources to ~~-~~ a Battery Energy Storage System ~~BESS~~: A Deep Learning – Based Control

Antonella Tannous, Reza Razi, Ferréol Binot, Bruno Francois

Univ. Lille, Arts et Métiers Institute of Technology, Centrale Lille, Junia, ULR 2697 - L2EP
F-59000 Lille, France
{antonella.tannous, ferreol.binot, bruno.francois}@centralelille.fr, reza.razi@ensam.eu

***Abstract*— Decarbonizing the energy sector requires integrating intermittent renewable energy sources. Such intermittency increases dependence on costly and environmentally detrimental power reserves provided by fast conventional generators. To maintain grid balance while keeping the energy cheap and decarbonized, grid operators must leverage flexible assets and make swift decisions. This paper introduces a novel deep learning-based controller to manage power reserves from an energy storage system. A deep neural network, trained on real-world data simulated through a physics-based tool, predicts power reserves to address rapid fluctuations. In supplementary to frequency droop controller, the intelligent controller regulates the frequency based on measured or forecasted power inputs. By combining predictive intelligence with real-time fast responsiveness, the proposed framework effectively manages the supply and demand fluctuations, enhancing grid stability while supporting decarbonization and cost efficiency. The framework is validated on an islanded microgrid through an innovative real-time structure using OPAL-RT and SPHEREA simulators.**

Keywords*— Grid balancing, Renewable energy sources, Energy storage, Deep learning, Real-time simulators.

I. Introduction

Over the years, traditional bulk power grids characterized by large conventional predictable and easily operated generators, as well as predictable demand, employ automated processes in control rooms to operate ahead of real-time. These processes are based on the swing equation, which models the power exchange between the mechanical rotor of synchronous generators and electrical grid. Therefore, explicit description of the physics-based mathematical functions and sensitive identification of parameters is unavoidable [1].

The COP28 World Climate Action Summit emphasized the importance of decarbonizing energy sources of bulk power grids to help limit the mean global temperature rise to 1.5ºC [2]. This decarbonization effort has led to a growing penetration of intermittent renewable energy sources (RES) at the distribution level, reflecting the distributed and intermittent nature of their resource availability. Additionally, decarbonization has also impacted the demand side, which now features greater variability and unpredictability due to the growing adoption of electric vehicles and battery systems. These new highly uncertain technologies integrated on both sides of the grid are inverter-interfaced technologies that reduce the overall grid's inertia and heightens the susceptibility to power imbalances and fast frequency drops [3]. As power grids become further complex and non-linear systems to operate, their dynamics are pushed closer to their operational limits, and their system parameters are not always accessible. Consequently, traditional model-based control schemes struggle to capture the grid's rapid dynamics and stochastic behaviour, as they rely on accurate system representation and parameter identification [4].

To address these challenges, it is essential to implement flexible system operations that enhance traditional physics-based approaches through continuous adaptive decision-making, to maintain grid balance at minimum economic and environmental costs. This requires leveraging model-free control approaches to enable efficient decisions, minimizing dependence on complex and hard-to-tune models.

As the world witnesses faster and easier access to data collected via smart metering devices along with increased computational capabilities, the adoption of machine learning (ML) methods in power grids is rapidly gaining momentum [5]. For active power balancing in microgrids, ML has emerged as a valuable tool for identifying system models, tuning controller parameters, generating supplementary control signals, or even replacing traditional model-based controllers entirely. Among ML approaches, reinforcement learning (RL) has been extensively applied due to its ability to learn through trial and error. This characteristic enables RL to handle the nonlinear, high-dimensional, and complex nature of microgrid control systems without requiring extensive offline datasets. For instance, [6] demonstrated the use of RL to replace model-based controllers, effectively reducing frequency deviations cause by wind power fluctuations, while other studies have explored its application in generating supplementary control signals for secondary frequency control [7, 8, 9]. However, RL faces several significant challenges such as scalability, as it is prone to the curse of dimensionality and increased complexity in exploration and training. Stability is another concern, with RL algorithms often exhibiting instability due to excessive exploration during learning. Additionally, issues related to the environment, security, and generalization further complicate the deployment of RL for microgrid control [10]. Moreover, RL can be challenging to implement and computationally expensive, particularly in real-time applications.

In contrast, supervised learning provides a more computationally efficient and stable alternative in certain scenarios. It has been extensively applied for fine-tuning frequency controller parameters [11]. Recent studies have explored the use of artificial neural networks (ANN) to fine-tune the inertia of a voltage source converter, enhancing frequency stability [12]. Authors in [13] developed an ANN-based controller to emulate the dynamics of a virtual synchronous generator to control the frequency. Most of these methods overlook the underlying causes of imbalances and rely solely on frequency measurements to balance the grid.

This work has been achieved within the framework of EE4.0 (Energie Electrique 4.0) project. EE4.0 is co-financed by European Union with the financial support of the European Regional Development Fund (ERDF), French State and the French Region of Hauts-de-France.

This paper overcomes the limitations of our previous work [14, 15] by introducing a deep learning-based controller designed to manage uncertainties in power production and demand within a microgrid. The proposed controller operates under realistic conditions, optimize operating costs and reducing CO_2 emissions. More specifically, a deep neural network (DNN)-based controller is developed and trained to predict power reserves at 5-minute intervals with 1-minute resolution. Leveraging power measurements or forecasts, it dynamically substitutes fuel-based power reserves with energy storage-based reserves, ensuring sustainable and efficient microgrid operation. The main contributions of this paper are as follows:

- Development of a real-time DNN-based control approach leveraging measured or very short-term forecasted power, instead of frequency measurements.
- Local integration of the intelligent controller alongside frequency droop control to achieve active power balancing in an islanded microgrid, enhancing system stability and performance.
- Quantitative evaluation of economic and environmental cost savings, achieved by efficiently managing power reserves from an energy storage system.
- Validation of the proposed control framework through an innovative setup using OPAL-RT and SPHEREA code execution hardware platforms.

The remainder of this paper is structured as follows. Section II presents a comprehensive overview of the proposed methodology. Section III details the case study employed for data collection and framework validation. Section IV describes the development and implementation of the proposed control framework. Section V focuses on the methodology for photovoltaic and load power forecasting. In Section VI, the performance assessment metrics for evaluating the proposed control framework are defined. Section VII provides an analysis and discussion of framework's results. Section VIII validates the outcomes through the real-time structure. Finally, Section IX concludes the paper with key insights and an outlook on future work.

II. Overview of The Proposed Methodology

Building trustworthy ML models involves addressing challenges in dataset creation and pre-processing, model training, assessment, and embedding, which can be tackled by integrating solutions into a comprehensive workflow [16].

Our general overview of the proposed methodology is described in Fig. 1~~Fig. 1~~. The proposed methodology follows a comprehensive workflow for developing and validating a DNN-based control solution for grid balancing. It begins with offline simulation, where a physics-based domain simulation of an islanded microgrid is conducted to generate a representative dataset (see Section III). This dataset undergoes sampling and pre-processing to ensure it is suitable for DNN model training (see Section IV.B). The next stage focuses on the design of the algorithm, involving hyper-parameter tuning, best model selection, and performance assessment to develop a robust control solution (see Sections IV.C and IV.D). In the online phase (see Section IV.A), the trained DNN model is implemented, in supplementary to the frequency droop control, for active power balancing. While the frequency droop control ensures frequency containment reserves (FCR), the DNN-based controller provides supplementary fast power reserves (secondary control). The DNN-based controller makes predictions of the supplementary minute-by-minute power reserves every 5 minutes, based on measured or forecasted power data (see Section V). Finally, the methodology is rigorously validated using real-time simulators, to evaluate the effectiveness and reliability of the proposed control framework (see Section VIII).

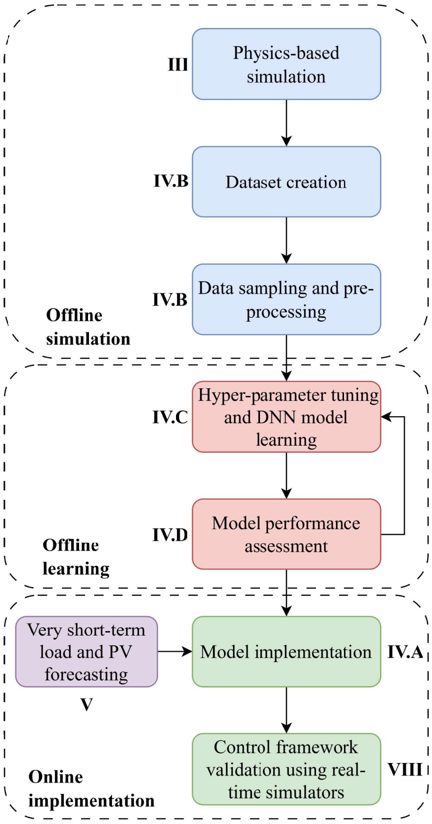

Fig. 1. General overview of the proposed methodology

III. Case Study: an Islanded Microgrid

The case study section is structured in two parts. The first part describes the microgrid configuration under study, while the second part specifies the data used for simulation.

A. *Microgrid architecture*

A simulation model of an islanded microgrid was developed on MATLAB/Simulink. The purpose of the simulation model is to 1) provide a database for the training phase and 2) test the proposed control strategy. The architecture of the microgrid is illustrated in Fig. 2~~Fig. 2~~. It consists of three layers: the physical, information, and control layers. The physical layer includes a 125 kW 3-phase Diesel Generator (DG), a 50 kW/kWh Li-ion Battery Energy Storage System (BESS), a 42.5 kW Photovoltaic (PV) system, and a group of residential loads with a peak electrical power of 85 kW. The information layer comprises smart meters that monitor and transmit data on PV generation, DG, and residential load power to the energy management system of the BESS. The control layer incorporates droop controllers to deliver FCR using both the DG and the BESS. Additionally, this layer features the proposed intelligent controller responsible for sending control signals to the BESS to ensure the provision of fast power reserves.

B. *PV and load power data*

The simulation is performed by using 186 days of historical PV and residential load data. The dataset is uniformly resampled to a consistent time resolution of one minute, with missing measurements addressed through polynomial interpolation. The PV power production data originates from a PV system installed

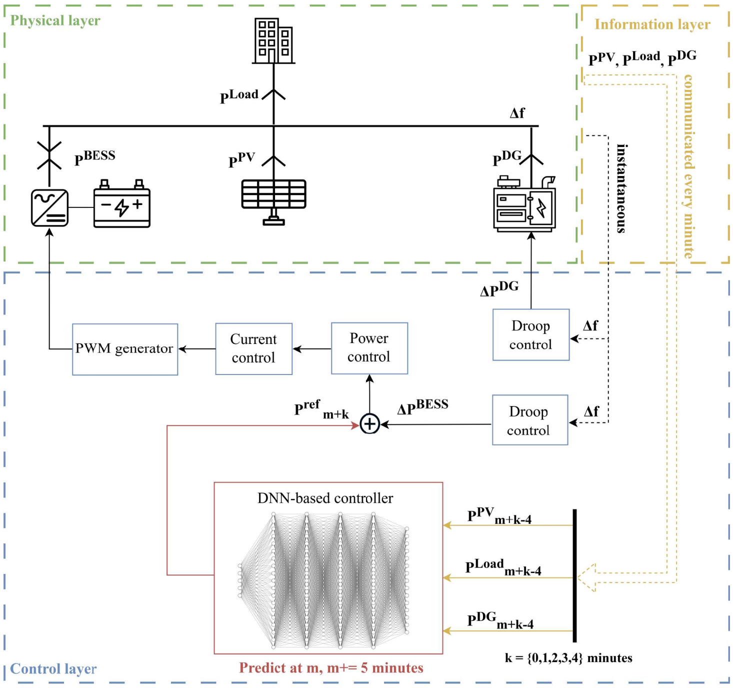

Fig. 2. The physical, information, and control layers of the microgrid

in northern France. This system experiences significant power fluctuations caused by fast-moving clouds. For the residential electrical load, the simulation incorporates the demand profile derived from [17]. Fig. 3~~Fig. 3~~ illustrates the PV and load profile on a random day.

IV. Proposed Control Framework

A. Brief overview of the proposed control framework

The proposed control framework (see Fig. 2~~Fig. 2~~) integrates a DNN-based controller supplementary to physics-based controllers to ensure active power balancing within the microgrid. Instantaneous FCR are provided by both the BESS and DG units through their frequency droop controllers (physics-based). These controllers, based on measured frequency deviation Δf and the same droop coefficient, instantaneously direct the allocation of power reserves ΔP^{DG} and ΔP^{BESS} from the DG and BESS units, respectively. The DNN-based controller utilizes as inputs minutely power measurements of PV, DG and load (P^{PV}_{m+k-4}, P^{DG}_{m+k-4}, and P^{load}_{m+k-4} with $k = \{0, 1, 2, 3, 4\}$ minutes), from 5 minutes prior the time of prediction m. Performance testing has also been conducted using short-term forecasted PV and load power values instead of

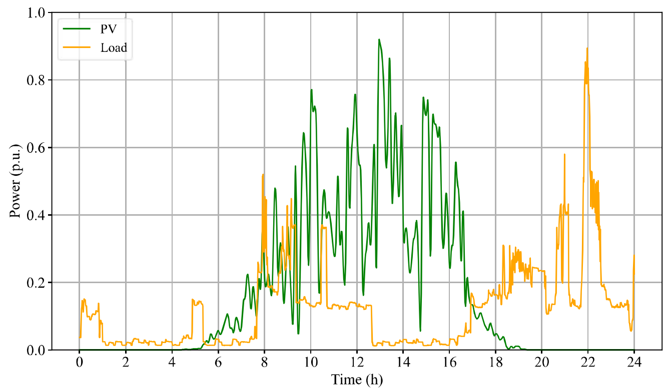

Fig. 3. PV and load demand profile on a random cloudy day

the measurements. Our DNN-based controller forecasts, at the minute m, the next 5 power reference values P^{ref}_{m+k} for the BESS, providing minute-by-minute predictions for the subsequent 5-minute interval. These forecasts are updated every 5 minutes, enabling dynamic scheduling of fast power reserves in the short term. Integrated into the energy management system of the BESS, the DNN-based controller anticipates fluctuations in PV and load power, substituting DG power reserves with BESS power reserves as needed. By offering a more reliable and flexible energy reserve, the controller enhances microgrid stability, reduces CO_2 emissions and operational costs.

B. Data creation, sampling and pre-processing

Supervised learning algorithms, such as deep learning, depend on datasets derived from either measurements or simulations. Simulation-based data generation provides the flexibility to create extensive datasets but is constrained by computational demands, particularly in non-linear systems or high-dimensional feature spaces [18]. As dimensionality increases, the sample size required for comprehensive coverage grows exponentially. To address this, targeted input selection can reduce the need for exhaustive sampling by focusing on outputs of interest.

In this study, the training process for the DNN leverages a simulation-based dataset comprising input and target values. The dataset is generated by simulating the same microgrid with fluctuating load and PV power inputs, deliberately excluding the BESS. This exclusion allows the DNN to learn the DG control policy in response to variations in load and PV power. The simulation spans 186 representative days with a 1-minute timestep to capture rapid fluctuations throughout the day and across different seasons.

The DNN within the BESS control system is designed to emulate the DG's droop controller during slow transients. To achieve this, the DNN is trained on the DG's slow power transient responses ΔP^{DG} sampled every minute, using input features f including PV power P^{PV}, load power P^{load}, and DG

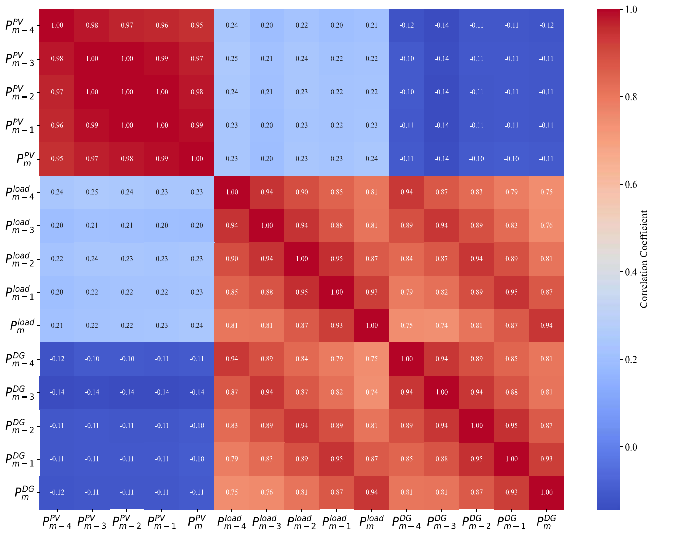

Fig. 4. Correlation study between input features

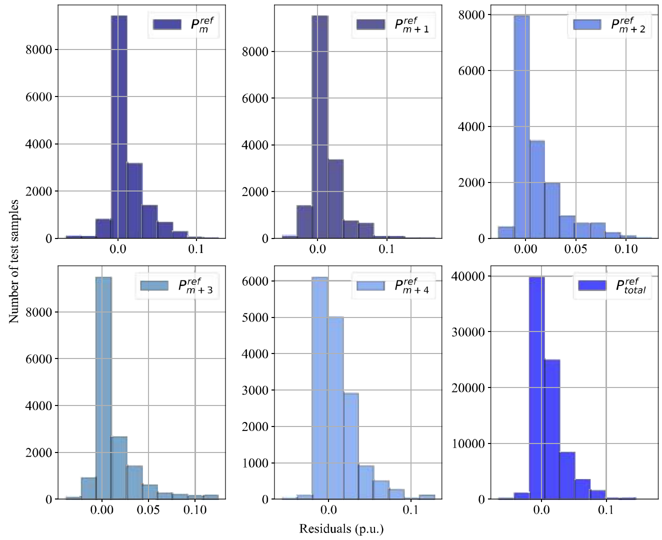

Fig. 5. Residual distribution of predicted output for test samples

power P^{DG}. These inputs enable the DNN to model the droop controller's behaviour under varying conditions effectively.

Fig. 4~~Fig. 4~~ depicts the correlation between the input features.

The diesel generator power P^{DG} shows a strong correlation (red – closer to 1) with P^{load} highlighting its key role in balancing demand when P^{PV} is insufficient. In contrast, P^{PV} exhibits weaker correlations (blue – closer to 0) with both P^{load} and P^{DG} because PV generation occurs only during daylight hours and is zero outside this period. However, both P^{PV} and P^{load} demonstrate strong temporal correlations within their respective time series, reflecting smooth and predictable very short-term trends (see Section V).

Prior to training, the dataset undergoes pre-processing. A 70/30 training-testing split is applied with a fixed random seed to ensure consistent conditions across models. Validation data, constituting 20% of training data, is crucial for assessing generalization and selecting optimal models. Pre-processing steps include standardizing input and target data, formatting to seven decimal places for precision, and handling the absence of values in the simulation-generated dataset.

C. Hyper-parameter tuning and DNN model selection

Overfitting occurs when a model performs well on training data but poorly on unseen data. To mitigate this, we monitor the validation error during training. Techniques include early stopping, where training halts if validation performance stops improving, and regularization (e.g., L1 or L2 penalties) to constrain model complexity and improve generalization. Additionally, hyperparameter tuning—adjusting parameters like model size, optimizer settings, or regularization strength—further enhances performance. Since hyperparameters affect model generalization in complex ways, they are typically optimized by using methods such as random search, grid search, Bayesian optimization, etc. [19].

Unlike grid search, which evaluates all possible combinations, random search explores a subset of configurations. Random search often leads to better results in less time, especially for high-dimensional parameter spaces.

In this study, we have chosen random search to explore the hyperparameter space by randomly sampling different combinations, evaluating up to 50 trials where each trial represents a unique set of hyperparameters (see Table I~~Table I~~). During each trial, the model is trained on the training dataset and validated on a subset, with performance measured by the validation loss after each epoch. The best hyperparameters are retrieved based on the lowest validation loss across all trials. The best model architecture (see Table II~~Table II~~) is rebuilt using the best hyperparameters.

D. DNN model training and performance assessment

Once the best model architecture is determined, the training process involves optimizing the model's weights and biases to minimize the loss function, thereby enhancing its predictive accuracy. The training process uses the Adam optimizer, which adapts the learning rates for each parameter, enhancing convergence. Additionally, the learning rate is dynamically reduced by 10% after 10 epochs to refine adjustments during later stages of training. Training is capped at 100 epochs but early stopping halts the process if the validation loss does not improve for 5 consecutive epochs, preventing overfitting. The resulting weights and biases represent the final learned parameters, which the model uses to make predictions. The mean squared error MSE is favoured for its ability to heavily penalize large errors, making the model more sensitive to significant deviations. The performance of the training and

Table I HYPER-PARAMETER OPTIONS

Hyper-parameter	Options
Number of layers	[3, 6] step size: 1
Nodes per layer	[16, 192] step size: 16
Activation function	Linear, ReLU, leaky ReLU, tanh, sigmoid
Leaky ReLU α	[0.01,0.3] step size: 0.1
Dropout rate	[0.2, 0.5] step size: 0.1
Learning rate	$[10^{-4}, 10^{-2}]$ logarithmic sample

Table II BEST DNN MODEL ARCHITECTURE

Layer Type	Number of Parameters
Dense ReLU	3,072
Batch normalization	768
Dropout 0.4 rate	0
Dense leaky ReLU	18,528
Dense leaky ReLU	9,312
Dense leaky ReLU	9,312
Dense linear	485

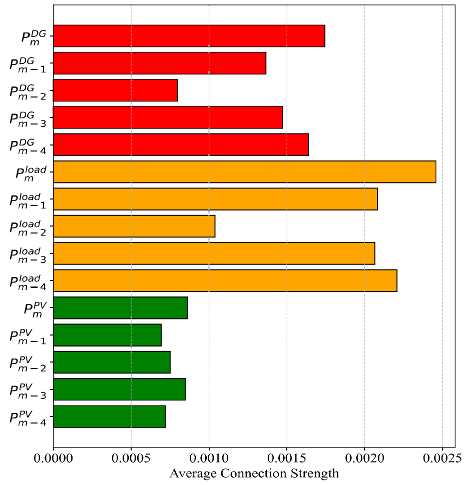

Fig. 6. Bar chart of the average connection strength of each input feature

validation processes is assessed by using MSE, as defined in (1~~(1~~):

$$\text{MSE} = \frac{1}{n} \cdot \sum_{i=1}^{n} (y_i - \hat{y}_i)^2 \tag{1}$$

where y_i and $\hat{y}_i$ denote the actual and predicted values, respectively, across the total number of samples n.

After 14 epochs, the training error reaches 0.0009, while the validation error stands at 0.001. A histogram of the test residuals, defined as $y_i - \hat{y}_i$ of the test samples, is illustrated in Fig. 5~~Fig. 5~~. The residual distributions for each output P^{ref}_{m+k} (with $k = \{0, 1, 2, 3, 4\}$) are tightly clustered around 0, suggesting the model performs well on unseen test data. Most residuals are slightly positive, suggesting a tendency to underestimate actual values, while the range of residuals spans from –0.05 to 0.15 per unit. The residuals of earlier outputs, such as P^{ref}_{m} and P^{ref}_{m+1} are more tightly distributed than later outputs, highlighting increased variability in predictions over the prediction horizon. Overall, the residuals for the total test samples P^{ref}_{total} confirm the model's reliability, showing minimal errors and few extreme outliers.

Fig. 6~~Fig. 6~~ highlights the impact of each input feature on the outputs through the average connection strength, calculated as the average magnitude of weights associated with each input feature across all connections. The most recent and delayed load power inputs, P^{load}_{m} and P^{load}_{m-4}, exhibit the highest connection strengths, while P^{load}_{m-2} demonstrates the weakest connection among the load features. This pattern is attributed to the volatile nature of the load demand. Even though PV generation has an important impact on the outputs during daylight hours, the PV power inputs show the lowest average connection strength, reflecting their minimal influence on the outputs, due to the absence of PV power generation outside daylight hours. Consequently, the DG power, which is more influenced by load power than PV power (see Fig. 4~~Fig. 4~~), displays moderate impact on the outputs. Fig. 7~~Fig. 7~~ further supports this analysis by displaying the dot product of the connection weights between each input and output feature. The colour intensity highlights the relative importance of each input, where warmer colours (yellow) indicate stronger weights. It is evident that P^{load}_{m} and P^{load}_{m-4} contribute significantly to the predictions $\hat{P}^{ref}_{m}$ and $\hat{P}^{ref}_{m+4}$.

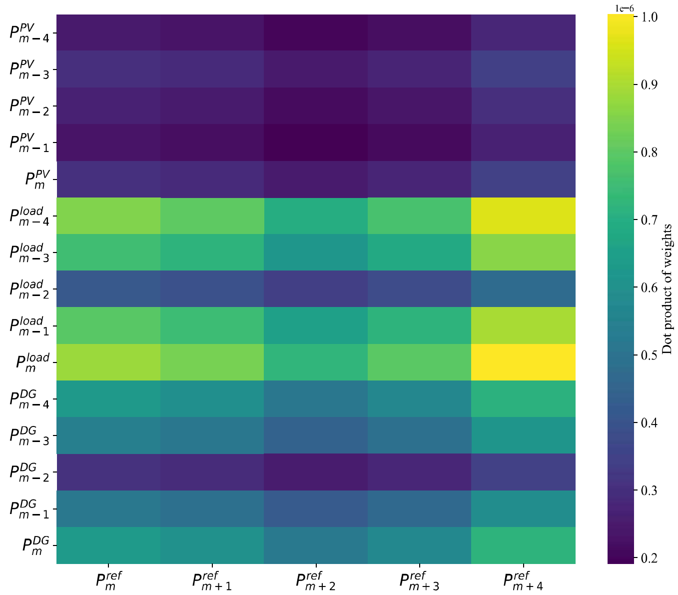

Fig. 7. Dot product of weights for all layers connecting each input feature to the outputs

V. Load and PV Forecasting

Load and PV forecasting is essential for anticipating future energy demands and supply over various time horizons, with very short-term forecasting (VSTF) focusing on predictions ranging from 1 minute to 1 hour ahead. VSTF is crucial for real-time decision-making, addressing very short-term random variations in supply and demand to maintain balance and minimize operational costs.

In this study, very-short term forecasting is performed at the time m to provide minute-by-minute forecasts for the subsequent 5 minutes. The forecasting error is evaluated using the mean absolute error MAE, given by (2~~(2~~):

$$\text{MAE} = \frac{1}{n} \cdot \sum_{i=1}^{n} |y_i - \hat{y}_i| \tag{2}$$

A. Very short-term load forecasting

Residential loads are the most challenging to forecast due to their volatility and non-linearity driven by human behaviour, making load VSTF especially difficult. Various methods like Time-Series analysis [20], Long-Short Term Memory [21], Polynomial Regression [22], and other hybrid combinations of methods [23] have been widely employed for VSTF of load demand. In this study, Polynomial Ridge Regression is chosen for its simplicity and computational efficiency. It generates minute-by-minute load predictions $\hat{P}^{load}_{m+k}$ for the next 5 minutes (with $k = \{0, 1, 2, 3, 4\}$), by leveraging historical data from the previous 5 minutes, specifically P^{load}_{m+k-4}.

Polynomial Ridge Regression is a type of regression technique that combines polynomial feature transformation with L2 regularization (Ridge) to prevent overfitting. By adding a penalty term R to the cost function, Ridge regression helps control the magnitude of the model's coefficients, ensuring its robustness to small fluctuations in the training data compared to standard polynomial regression. The model captures complex relationships in data by using polynomial features described in (3~~(3~~) for each value of k:

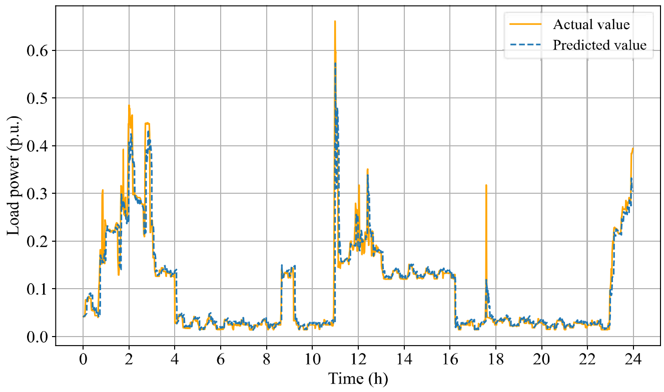

Fig. 8. Actual versus predicted load power on a random day

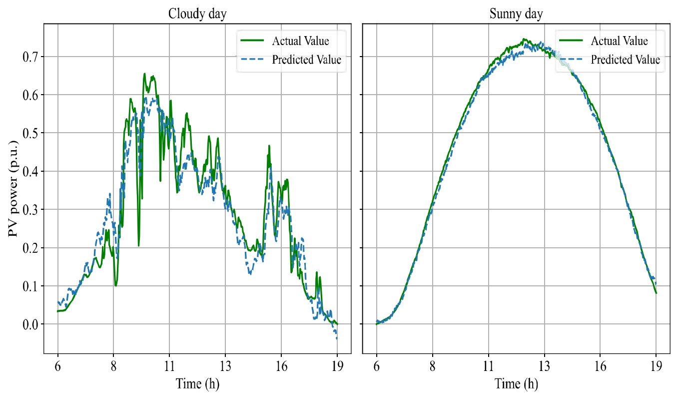

Fig. 9. Actual versus predicted PV power on a cloudy and sunny day

$$\widehat{P}^{load}_{m+k} = \beta_0 + \sum_{d=1}^{D} \beta_d \cdot \left(P^{load}_{m+k-4}\right)^d \tag{3}$$

where β_0 is the intercept term, and β_d are the coefficients corresponding to the d-th degree terms in the polynomial of degree D. The hyperparameter D will be next optimized.

The dataset is partitioned as follows: 70% for training (including 10% for validation) and 30 % for testing. A grid search is conducted to identify the optimal hyperparameters for a Polynomial Ridge Regression model. This process involves performing 5-fold cross-validation for each hyperparameter combination, calculating the average negative MSE across all folds. The hyperparameters yielding the lowest average negative MSE are selected as the optimal configuration, minimizing the Polynomial Ridge Regression objective function $L(\beta)$ as described in (4~~(4~~) and (5~~(5~~):

$$L(\beta) = \frac{1}{n} \cdot \sum_{m=5,\ m+5,\dots}^{n} \left(P^{load}_{m+k} - \widehat{P}^{load}_{m+k}\right)^2 + R \tag{4}$$

where

$$R = \lambda \cdot \sum_{d=1}^{D} \beta_d^{\,2} \tag{5}$$

The analysis identifies a polynomial degree of 3 and a ridge regularization strength λ of 0.01 as the optimal parameters. The values of β_0 and β_d are determined by the regression process itself. The resulting model achieves a MAE of 2% on unseen data. Fig. 8~~Fig. 8~~ showcases the actual versus predicted load demand on a random day.

B. *Very short-term Photovoltaic forecasting*

Very short-term solar forecasting, also known as intra-hour solar forecasting, refers to the prediction of PV power generation within the same hour, typically at higher time resolutions such as every 5, 10, or 15 minutes. Several methods have been developed for this task, including time-series models like ARIMA, statistical and machine learning models, and advanced image-based techniques. Recent advances leverage satellite and sky images with convolutional neural networks (CNNs) and long short-term memory networks. Combining ground-based sky imagery with historical PV outputs in specialized CNN architectures has shown promise, particularly for handling complex cloud movements and short prediction horizons [24].

This study builds upon the PV forecasting approach presented in [25], with a key modification reducing the forecasting horizon from 15 minutes to 5 minutes. The proposed hybrid model combines image-based and temporal features using a CNN architecture and fully connected layers. It processes a sequence of images from a 360-degree fisheye camera, concatenated along the colour channel, combined with the measured PV power from 5 minutes prior P^{PV}_{m+k-4}, which is integrated mid-network.

The hybrid model, illustrated in Fig. 10~~Fig. 10~~ predicts PV power output $\widehat{P}^{PV}_{m+k}$ for the upcoming 5 minutes by leveraging spatial features from image sequences and numerical PV power data. The input consists of 5 image sequences, each with dimensions 64×64 pixels with 3 color channels RGB (Red-Green-Blue), passed through two convolutional layers with 24 and 48 filters, respectively. Each convolutional layer is followed by batch normalization, ReLU activation, and max pooling. The extracted spatial features are then flattened and concatenated with P^{PV}_{m+k-4}. This fused feature representation is processed through two fully connected layers, each containing 1024

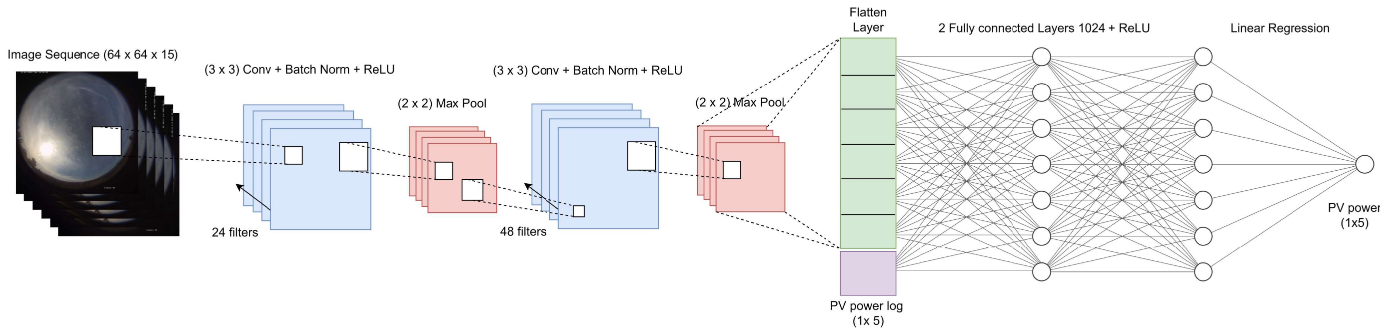

Fig. 10. Hybrid CNN model with PV power log to predict PV power

neurons with ReLU activation. The model concludes with a linear regression layer to predict PV power outputs $\widehat{P}^{PV}_{m+k}$. The architecture incorporates strong regularization techniques, such as dropout and batch normalization, to enhance generalization and effectively predict short-term PV power variations. The hybrid model achieves a 2.12% MAE on previously unseen sunny days and a 7.78% MAE on previously unseen cloudy days. Fig. 9~~Fig. 9~~ showcases the actual versus predicted PV power on a cloudy and sunny day.

VI. Performance Evaluation Metrics

The performance of the proposed control strategy is evaluated over a period T of 5 minutes, through three interrelated metrics: technical, environmental, and economic. The technical performance is assessed by analysing frequency stability using the Integral of Frequency Deviation (IFD). The environmental impact is quantified by calculating the total mass of CO_2 emissions generated during the operation of the DG. Finally, the economic aspect is evaluated by determining the costs incurred from fuel consumption by the DG and the associated taxes on emissions. This integrated evaluation framework ensures a holistic assessment of the control strategy, addressing reliability, sustainability, and cost-efficiency.

A. Integral of frequency deviation

The IFD is a robust and intuitive metric for analysing frequency stability in power grids with a high share of RES. The IFD metric, defined in (6~~(6~~), evaluates the cumulative magnitude of the deviation from the nominal frequency $f_{nominal}$ (50 Hz in this case) over the specified period T.

$$\mathrm{IFD} = \int_0^T |f(t) - f_{nominal}|dt \tag{6}$$

B. Environmental costs

The operating CO_2 emissions within the microgrid depend on the DG's fuel consumption denoted as l_{fuel} [L/kWh] and can be formulated as a quadratic function of the DG power P^{DG}. The coefficients of this function are determined through curve fitting of the fuel consumption chart [26] (see Table III~~Table III~~), as described in (7~~(7~~):

$$l_{fuel} = (-5\times 10^{-4})\cdot {P^{DG}}^2 + 0.3\cdot P^{DG} + 2.4 \tag{7}$$

Given that a DG releases 2.68 kg of CO_2 per Liter of fuel consumed [27], the total emitted mass m_{CO_2} [kg] of CO_2 can be represented by (8~~(8~~). This equation is as a function of DG power evolution, accounting for the engine delay T_e with a specified value of 0.03 seconds [28].

$$m_{CO_2} = \int_0^T 2.68/Te\cdot e^{-t/Te}\cdot l_{fuel}\, dt \tag{8}$$

Table III Fuel Consumption Chart for the Specified DG

DG Power [kW]	Fuel Consumption [L/h]
50% load	21.90
75% load	30.30
100% load	37.80

C. Economic costs

The total operating costs c_{eco} can be formulated by incorporating both the cost of consumed diesel and the tax associated with the mass of CO_2 emitted, as depicted in (9~~(9~~). The considered cost of a Liter of diesel is 1.865 €, while the CO_2 emission tax is 44.6 € per ton [3].

$$c_{eco} = 44.6/1000\cdot m_{CO_2} + 1.865\cdot \int_0^T l_{fuel}\, dt \tag{9}$$

VII. Results and Discussion

In this section, the proposed control framework is evaluated using an islanded microgrid model developed in MATLAB/Simulink (see Fig. 2~~Fig. 2~~). The primary objective is to assess the framework's performance under conditions closely resembling real-world operating conditions, characterized by continuous fluctuations in PV and load power. The evaluation compares the framework, which integrates the DNN-based controller with the BESS and the DG frequency droop controllers, across two scenarios (see Fig. 11~~Fig. 11~~): one using historically measured power inputs of Section V (red curve – control scenario 1) and the other using forecasted power inputs (green curve – control scenario 2). The analysis also includes comparisons with a scenario involving only the DG and BESS droop controllers (blue curve – control scenario 3) and another scenario relying solely on the DG droop controller (yellow curve – control scenario 4).

The simulation is carried out over a 10-minute duration. During the initial five minutes, the DNN-based controller does not generate BESS reference power, as historical power measurements are required to initialize its algorithm. These measurements are not available at the start of the simulation and are instead collected during the first 5 minutes. Therefore, the results presented in Fig. 11~~Fig. 11~~ focus on the period from 4.5 to 10 minutes only, highlighting the performance of the proposed control framework starting minute 5.

During the initial 5 minutes, only the DG droop controller (yellow curve) responds to the frequency deviation Δf of 0.21

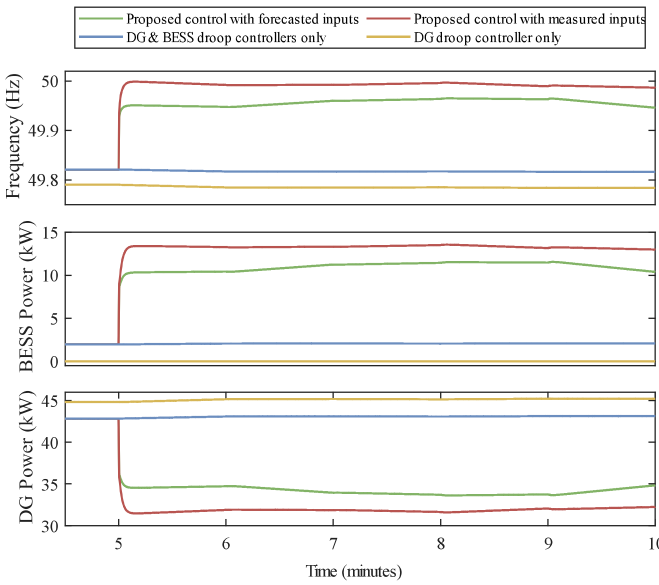

Fig. 11. Microgrid frequency, BESS and DG active power under four control scenarios, for continuously fluctuating PV and load power

Hz by supplying FCR. In contrast, the red, green, and blue curves state the contribution of both the BESS and DG droop controllers to the frequency regulation according to their respective power capacities and droop coefficients. As expected, the microgrid frequency regulation is more effective when the BESS provides an additional 2 kW of FCR, thereby improving overall system stability. This contribution not only enhances frequency control but also reduces operational costs and emissions by displacing DG-based reserves.

After 5 minutes ($m = 5$), the DNN-based controller generates five predicted BESS reference values P_{m+5}^{ref} for both the red and green curves. These predictions will increase the provision of supplementary fast power reserves from the BESS, mitigating and replacing the reserves provided by the DG. The VSTF exhibit a total error of 6% on both PV and load power for this test, which affects the accuracy of the DNN's predictions when relying on forecasted power inputs. The DNN-based controller utilizing measured inputs (red curve) outperforms the one using forecasted inputs (green curve). Specifically, the control framework in the red curve most effectively maintains the microgrid frequency closest to 50 Hz, while further minimizing DG power consumption.

Table IV~~Table IV~~ presents the performance evaluation metrics for each scenario over the 5-minute period. The DNN-based controller with measured inputs (control scenario 1) achieves the lowest values for the IFD, m_{CO_2} and c_{eco} metrics. Conversely, scenario 4, which only uses the DG droop controller, exhibits the highest values for these metrics. Scenario 1 reduces the IFD metric by 0.18, 0.87, and 1.04 Hz·min compared to scenarios 2, 3, and 4, respectively. Furthermore, scenario 1 results in a reduction of the mass of CO_2 emissions m_{CO_2} and operating costs c_{eco} by 5.3%, 21.05%, and 30.3% compared to scenarios 2, 3, and 4, respectively.

The DNN-based controller with forecasted inputs demonstrates an improvement in system performance by 0.69 Hz·min and a reduction in costs and emissions by 15.9% compared to scenario 3. Additionally, it shows an improvement of 0.86 Hz·min and a reduction in costs and emissions by 23.7% compared to scenarios 4. However, its effectiveness depends on the accuracy of the forecasted power inputs. Smaller discrepancies between actual power measurements and forecasts lead to better outcomes for the DNN-based controller in scenario 2. Scenarios 1 and 2 significantly improve on the three indicators used, compared with scenarios 3 and 4. Scenario 1 is indeed the most accurate, but measurements are not always available. The use of load and PV prediction algorithms are therefore good tools for improving the control framework's data input.

Table IV PERFORMANCE EVALUATION METRICS

Control scenario	IFD [Hz.min]	m_{CO_2}[kg]	c_{eco} [€]
1 (red curve)	0.04	2.557	1.89
2 (green curve)	0.22	2.693	1.99
3 (blue curve)	0.91	3.214	2.38
4 (yellow curve)	1.08	3.332	2.47

VIII. VALIDATION OF THE CONTROL FRAMEWORK USING AN INNOVATIVE REAL-TIME STRUCTURE

The performance and effectiveness of the proposed control framework are validated by using an innovative setup featuring two advanced real-time simulators, interconnected via robust communication protocols, as depicted in Fig. 12~~Fig. 12~~. The OPAL-RT simulator is employed to model the physical and control layers of the microgrid using MATLAB/Simulink software. Simultaneously, the SPHEREA simulator is utilized to execute the DNN algorithm for predicting future setpoints, leveraging U-Test software and Python programming for algorithm implementation. A bidirectional communication protocol—Message Queuing Telemetry Transport (MQTT)—ensures seamless and reliable data exchange between the simulators, facilitating the synchronization of their operations.

Every 5 minutes, the OPAL-RT simulator transmits load, PV and DG power measurements to the SPHEREA simulator. The DNN model in SPHEREA predicts the reference power P_{ref} for the next 5 minutes and relays this information to the BESS's control layer.

To visualize and analyse the results in real-time, a Supervisory Control and Data Acquisition (SCADA) system is

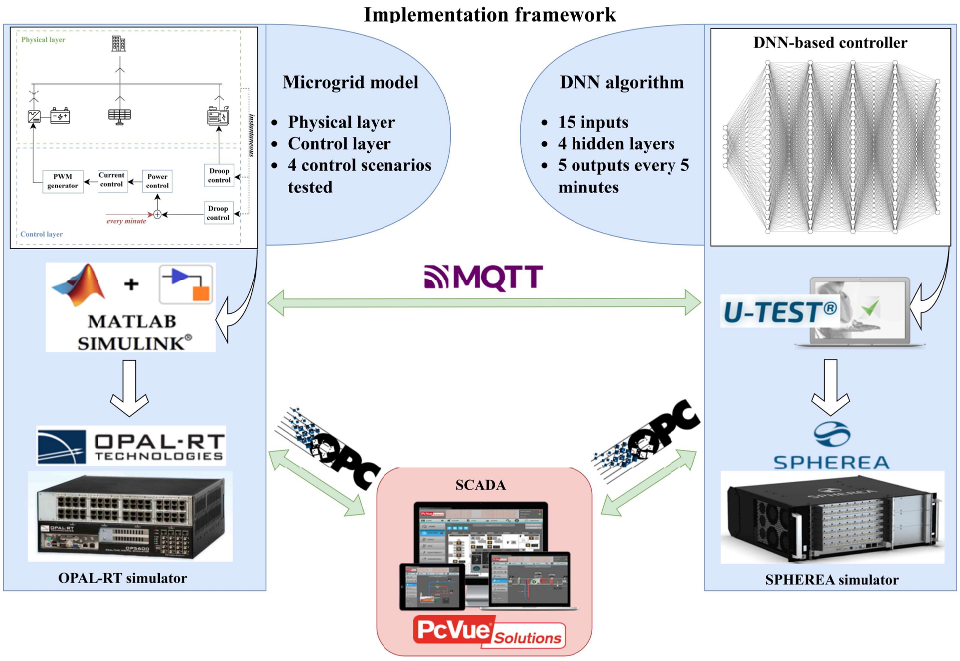

Fig. 12. Hardware and software organization of the real-time structure

implemented using PcVue software, which is communicating with the simulators via the Open Platform Communications (OPC) protocol. The SCADA system provides a user-friendly interface with advanced real-time monitoring and analytical capabilities. This interface enables users to observe and adjust the current state of the process dynamically. Key features included:

- Switching between control scenarios for comparative performance evaluation.
- Monitoring critical metrics such as system frequency, as well as the power outputs of DG and BESS units.
- Detailed insights into the evolution of operational parameters, including fuel consumption, associated costs, and emissions for each control strategy.

A key advantage of the real-time simulation environment is its computational efficiency compared to conventional PC-based simulations. While the real-time structure runs simulations at actual system speed, executing the same simulation on a high-performance PC equipped with a 12th Gen Intel® Core™ i7-12700H processor (2.3 GHz) and 32 GB of RAM takes almost eight times longer.

IX. Conclusions

This paper addresses the challenge of maintaining grid balance amidst the stochastic and intermittent nature of RES and the growing unpredictability of load demand. A novel DNN-based control framework is proposed to dynamically manage power reserves from a BESS, complementing frequency droop controllers. Unlike conventional frequency-based approaches, the DNN-based controller leverages historical power measurements or very short-term forecasts to provide fast, clean, and cost-effective power reserves. The framework is validated using realistic load and PV power profiles within an innovative real-time setup that closely emulates real-world operating conditions.

The proposed approach demonstrates significant advantages in frequency regulation, economic efficiency, and environmental impact. Compared to a control framework that relies solely on droop controllers, the DNN-based controller effectively reduces dependence on the DG, leading to lower CO_2 emissions and operational costs. The results confirm that using historically measured power inputs achieves the most accurate performance, maintaining microgrid frequency closest to 50 Hz while minimizing DG power consumption. Furthermore, the integration of very short-term forecasting provides a viable alternative when real-time measurements are unavailable, highlighting the adaptability of the proposed method.

Despite its promising results, this study has some limitations. The accuracy and reliability of the proposed method depend on the availability and quality of the data used for training and forecasting. Forecasting uncertainty can introduce deviations in power reserve predictions, affecting control performance. Additionally, the framework assumes the availability of sufficient power reserves from the BESS, which may not always be guaranteed under extreme operating conditions. Finally, real-time implementation may face computational constraints, including hardware limitations and communication delays, which require further investigation for large-scale deployment.

As a continuation of this work, we propose an investigation into the use of Importance Sampling to optimize the selection of a sampling distribution, focusing on identifying and prioritizing informative samples [18]. This approach aims to reduce the offline computation time and evaluate whether the DNN can sustain robust performance when trained on a smaller available dataset. Another key aspect is evaluating the controller's ability to maintain grid balance in the absence of conventional droop controllers, thus exploring its potential to operate autonomously under decentralized conditions. Finally, we plan to extend the study to a larger microgrid with multiple distributed RES and energy storage systems, employing a distributed learning approach to enable coordinated control among storage units and ensure grid stability in more complex systems. These directions aim to enhance the scalability, adaptability, and practical applicability of DNN-based controllers.

~~This paper addresses the challenge of maintaining grid balance amidst the stochastic and intermittent nature of RES and the growing unpredictability of load demand. A DNN algorithm is trained on simulated data and integrated into a control framework to operate in supplementary to frequency droop controllers. Based on historical power measurements or power forecasts, the DNN-based controller dynamically adjusts the power references of a BESS to deliver fast, clean, and cost-effective power reserves. The performance of the DNN-based controller is evaluated by using realistic load and PV power profiles within a real-time structure, effectively emulating real-world operating conditions.~~

~~As a continuation of this work, we propose an investigation into the use of Importance Sampling to optimize the selection of a sampling distribution, focusing on identifying and prioritizing informative samples [18]. This approach aims to reduce the offline computation time and evaluate whether the DNN can sustain robust performance when trained on a smaller available dataset. Additionally, since the DG power is inherently influenced by PV and load variations, we aim to analyse the impact of excluding DG power as an input feature to determine its necessity. Another key aspect is evaluating the controller's ability to maintain grid balance in the absence of conventional droop controllers, thus exploring its potential to operate autonomously under decentralized conditions. Finally, we plan to extend the study to a larger microgrid with multiple distributed RES and energy storage systems, employing a distributed learning approach to enable coordinated control among storage units and ensure grid stability in more complex systems. These directions aim to enhance the scalability, adaptability, and practical applicability of DNN-based controllers.~~

References

[1] O. Stanojev, Y. Guo, P. Aristidou, and G. Hug, "Multiple Ancillary Services Provision by Distributed Energy Resources in Active Distribution Networks," in *IREP 2022 - 11th Bulk Power Systems Dynamics and Control Symposium*, 2022, pp. 1-11.

[2] *United Nations Framework Convention on Climate Change*. Accessed: Mar. 14, 2024. [Online]. Available: http://unfccc.int/decisions.

[3] M. I. Saleem, S. Saha, and T. K. Roy, "A frequency stability assessment framework for renewable energy rich power grids," *Sustainable Energy, Grids and Networks*, vol. 38, pp. 101380-101396, 2024.

[4] O. Stanojev, U. Markovic, P. Aristidou, G. Hug, D. Callaway, and E. Vrettos, "MPC-Based Fast Frequency Control of Voltage Source Converters in Low-Inertia Power Systems," *IEEE transactions on power systems*, vol. 37, no. 4, pp. 3209–3220, 2022.

[5] A. Tannous, R. Razi, F. Binot, and B. Francois, "A review of self-learning and adaptive techniques for grid balancing," in *Symposium de Génie Electrique*, 2023, pp. 1–6.

[6] Z. Yan and Y. Xu, "Data-Driven Load Frequency Control for Stochastic Power Systems: A Deep Reinforcement Learning Method with Continuous Action Search," *IEEE transactions on power systems*, vol. 34, no. 2, pp. 1653–1656, 2019.

[7] M. Adibi and J. Van der Woude, "Secondary frequency control of microgrids: An online reinforcement learning approach," *IEEE Trans. Autom. Control*, vol. 67, no. 9, pp. 4824–4831, Sep. 2022.

[8] M. H. Khooban and M. Gheisarnejad, "A novel deep reinforcement learning controller-based type-II fuzzy system: Frequency regulation in microgrids," *IEEE Trans. Emerg. Topics Comput. Intell.*, vol. 5, no. 4, pp. 689–699, Aug. 2021.

[9] A. Venkataramanan and A. Mehrizi-Sani, "Reinforcement Learning-Based Transient Response Shaping for Microgrids," in *IREP 2022 - 11th Bulk Power Systems Dynamics and Control Symposium*, 2022, pp. 1-9.

[10] B. She, F. Li, H. Cui, J. Zhang, and R. Bo, "Fusion of Microgrid Control with Model-free Reinforcement Learning: Review and Vision," *IEEE transactions on smart grid*, vol. 14, no. 4, pp. 3232–3245, 2023.

[11] F. Habibi, S. Shokoohi, and H. Bevrani, "Designing a self-tuning frequency controller based on ANN for an isolated microgrid," in *Int. Symp. On Smart Grid Operation and Control*, 2012, pp. 1–12.

[12] F. Yao, J. Zhao, X. Li, L. Mao, and K. Qu, "RBF Neural Network Based Virtual Synchronous Generator Control with Improved Frequency Stability," *IEEE transactions on industrial informatics*, vol. 17, no. 6, pp. 4014–4024, 2021

[13] H. Issa, V. Debusschere, L. Garbuio, P. Lalanda, and N. Hadjsaid, "Artificial intelligence-based controller for grid-forming inverter-based generators," in *Innovative Smart Grid Technologies Conf.*, 2022, pp. 1–6

[14] A. Tannous, R. Razi, F. Binot, B. Francois, "Artificial neural network-based fast power reserve control for active power balancing," *Int. Conf. Electrimacs*, 2024, pp. 1–6.

[15] A. Tannous, R. Razi, F. Binot, B. Francois, "Short-Term Scheduled Power Reserve: An Artificial Neural Network Approach," *CIRED 2024 Vienna Workshop*, 2024, pp. 1–6.

[16] J. Stiasny, S. Chevalier, R. Nellikkath, B. Sævarsson, and S. Chatzivasileiadis, "Closing the Loop: A Framework for Trustworthy Machine Learning in Power Systems," in *IREP 2022 - 11th Bulk Power Systems Dynamics and Control Symposium*, 2022, pp. 1-21.

[17] G. Hebrail and A. Berard. "Individual Household Electric Power Consumption," UCI Machine Learning Repository, 2006. [Online]. Available: https://doi.org/10.24432/C58K54.

[18] C. Hamon, M. Perninge, and L. Söder, "An importance sampling technique for probabilistic security assessment in power systems with large amounts of wind power," *Electric power systems research*, vol. 131, pp. 11–18, 2016.

[19] L. Yang and A. Shami, "On hyperparameter optimization of machine learning algorithms: Theory and practice," *Neurocomputing*, vol. 415, pp. 295–316, 2020.

[20] L. C. M. de Andrade and I. N. da Silva, "Very Short-Term Load Forecasting Based on ARIMA Model and Intelligent Systems," in *2009 15th International Conference on Intelligent System Applications to Power Systems*, IEEE, 2009, pp. 1–6.

[21] K. Li, W. Huang, G. Hu, and J. Li, "Ultra-short term power load forecasting based on CEEMDAN-SE and LSTM neural network," *Energy and buildings*, vol. 279, pp. 112666- 112681, 2023.

[22] V. K. Vats, S. Rai, D. Bharti, and M. De, "Very Short-Term, Short-Term and Mid-Term Load Forecasting for Residential Academic Institute: A Case Study," in *2018 4th International Conference on Computing Communication and Automation (ICCCA)*, IEEE, 2018, pp. 1–6.

[23] M. Zhang *et al.*, "Accurate ultra-short-term load forecasting based on load characteristic decomposition and convolutional neural network with bidirectional long short-term memory model," *Sustainable Energy, Grids and Networks*, vol. 35, pp. 101129- 101143, 2023.

[24] Y. Chu, M. Li, C. F. M. Coimbra, D. Feng, and H. Wang, "Intra-Hour Irradiance Forecasting Techniques for Solar Power Integration: A Review," *iScience*, vol. 24, no. 10, pp. 1-50, 2021.

[25] Y. Sun, V. Venugopal, and A. R. Brandt, "Short-term solar power forecast with deep learning: Exploring optimal input and output configuration," *Solar energy*, vol. 188, pp. 730–741, 2019.

[26] Ministère de l'economie, des finances, et de la souveraineté industrielle et numérique, "Guide 2024 sur la fiscalité des énergies", pp. 7

[27] Caterpillar Diesel Generator Sets D125 GC. [Online]. Available: http://www.cat.com/en_GB/products/new/power-systems/electric-power/diesel-generator-sets/106020.html.

[28] M. Khursheed, M.A. Mallick, and A. Iqbal, "Performance analysis of closed loop control of diesel generator power supply for base transceiver (BTS) load," *International Journal of Innovative Technology and Exploring Engineering (IJITEE)*, vol. 8, pp. 2483-2495, 2019.